Contents

1 Introduction **1**

1.1 Phase slip phenomenon in 1D superconductors 4

1.1.1 Time dependent Ginzburg-Landau theory 4

1.1.2 Phase slip mechanisms 7

1.1.3 Application of the Ginzburg-Landau theory 11

1.2 Superconducting films: flux flow instability and formation of phase slip lines 13

1.3 Details of the numerical approach 16

2 Critical currents of the phase-slip process in the presence of electromagnetic radiation, Rectification for time asymmetric ac signal **19**

2.1 Introduction 19

2.2 Theoretical model 20

2.3 numerical results 21

2.3.1 A) Symmetric ac signal 21

2.3.2 B. asymmetric ac signal 28

2.4 Discussion 29

3 Phase slip phenomena in NbN superconducting wires with leads **33**
3.1 Introduction 33
3.2 Experimental results 34
3.3 Theoretical model 36
3.4 Numerical results 38
3.5 Conclusion 41

4 Finite size effect on the resistive state in a mesoscopic type-II superconducting stripe **43**
4.1 Introduction 43
4.2 Theoretical model 44
4.3 Finite size effect on the resistive state 46
4.4 Effect of γ on the formation of phase slip lines 49
4.5 The influence of normal contacts 52
4.6 Hysteretic behavior 53
4.7 Conclusion 56

5 The break-up of the vortex structure in a mesoscopic wire containing a constriction **57**
5.1 Introduction 57
5.2 Theoretical model 58
5.3 Results and discussions 60
5.4 Conclusion 62

6 Summary **63**

7 Sumenvatting **67**

List of abbreviations **71**

References **75**

Curriculum Vitae **82**

List of publications **84**

1

Introduction

Two important properties of superconducting materials – zero electrical resistance [1] and perfect diamagnetism [2] – makes them very promising in practical applications. However, the existence of superconducting state is restricted by three main parameters: the critical temperature T_c, the critical current j_c and the critical magnetic field H_c. Intense efforts have been made to increase these critical parameters and enlarge the boundaries of the superconducting state in the (T, j, H)-space (see Fig. 1.1). As temperature is concerned, a particular breakthrough was the discovery of high temperature superconductors in 1986 in the $La_{2-x}(Ba,Sr)_xCuO$ compounds by J.G. Bednorz and K.A. Müller [3]. At present a record T_c of 164 K under 30 GPa pressure belongs to this class of superconductors [4]. In addition, the introduction of periodic arrays of artificial pinning centers leads to shifts of the $T_c(H)$ phase boundary towards higher temperatures compared to non-patterned films (see e.g. Ref. [5]). The presence of these pinning sites gives rise to matching effects when the vortex lattice is commensurate with the array of pinning sites, which leads to a considerable increase of the critical current of superconductors.

At the critical current a superconducting sample generally does not enter the fully normal conducting state, but usually exhibits a finite resistance. The nature of the resistive state in superconductors attracts much attention, since it involves fundamental phenomena and advanced concepts such as the mechanisms of high-T_c superconductivity [6], thermal fluctuations [7, 8], macroscopic

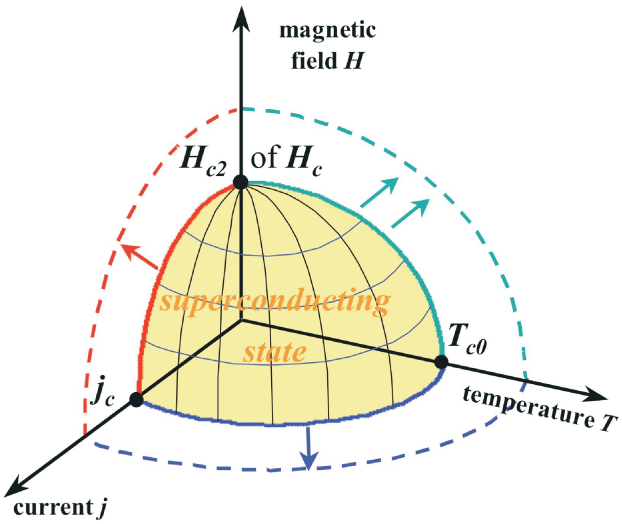

FIG. 1.1: Schematic representation of the expansion of the critical parameters.

quantum tunneling [9], coherence [10], topological excitations (e.g. phase-slips, vortices), phase disordering [11] etc. Therefore, understanding the resistive state is important for the advancement of fundamental science and the development of novel applications.

The main objective of this thesis is to study the response of mesoscopic samples (samples with size comparable to characteristic length scales – the coherence length ξ and the penetration depth λ) to applied *as* and *dc* currents. The outline of the thesis is as follows:

Chapter 1 starts with the description of the nature of a phase slip phenomenon in 1-dimensional superconductors including phase slip center (PSC) manifestation. We discuss the dynamics of vortices in 2D samples and show the formation of phase slip lines (PSL) under the external current ad magnetic field. Our theoretical approach will be given, which is based on the time-dependent Ginzburg-Landau (TDGL) theory.

In **Chapter 2**, we study theoretically the effect of time symmetric and asymmetric electromagnetic radiation on the phase-slip process in superconducting wires. Such asymmetric signal (with zero *dc* component) may lead to a finite voltage in the system (*i.e.*, ratchet effect). With adding positive *dc* current to the original *ac* current, we increase the time during which the current is positive and it raises the number of positive phase slip events.

In **Chapter 3**, transport properties of a superconducting NbN nanowires with attached superconducting contacts are studied both theoretically and experimentally. Different attached leads in experimental samples allowed us to

measure current-voltage (I-V) characteristics of different segments of the wire independently. The experimental results show that with increasing the length of the segment the number of jumps in the I-V curve increases indicating an increasing number of phase-slip phenomena. However, these finite jumps in the I-V curve disappears in current sweep down regime, although clear hysteresis in clearly obtained. The interpretation of the experimental results are supported by theoretical simulations that are based on the time dependent Ginzburg-Landau theory, coupled to the heat equation.

In next chapter (**Chapter 4**), we study the creation of phase slip lines and the interplay with a vortex lattice in finite size superconducting thin films. We found that with increasing transport current phase slip lines appear across the sample leading to distinct jumps in the current-voltage characteristics, which has a hysteretic behavior. When the magnetic field is applied to the system, the moving vortex lattice becomes rearranged by the external current and fast and slow moving vortex channels are formed. Curved vortex channels are also observed near the normal contacts. We found the remarkable result that the normal state transition current increases at small applied magnetic field as compared to the one at zero magnetic field. This effect becomes more pronounced for larger values of the γ parameter in the GL formalism. We explained this unusual "field-induced" increase of the critical current by the nonuniform distribution of the currents in the sample.

Vortex states in a nonuniform rectangular wire under the parallel magnetic field is studied in **Chapter 5**. We found that nonsymmetric vortex states may exist in our system as metastable states, which we related to surface barrier effects. The surface barrier for vortex entry/exit is responsible for the strong hysteresis which is an intrinsic property of our wire.

1.1 PHASE SLIP PHENOMENON IN 1D SUPERCONDUCTORS

One-dimensional superconductors have been expected to be the most simple system one can imagine for the investigation of the current-induced breakdown of superconductivity. However, measurements of voltage-current characteristics at fixed temperature T of microbridges at the critical current j_c do not show the direct transition into the fully normal conducting state. Instead, a large transition width from the first onset of voltage to the complete normal state has been usually obtained, as shown e.g. in Fig. 1.2. In this transition region the voltage increases in a series of regular voltage jumps. Moreover, electromagnetic radiation was detected in such samples [12] resembling the Josephson effect. These facts indicated to nonequilibrium and nonstationary nature of the formation of resistive state in such small samples.

1.1.1 Time dependent Ginzburg-Landau theory

Before considering the mechanism leading for such finite resistive state, let us briefly describe the time-dependent Ginzburg-Landau theory, which can

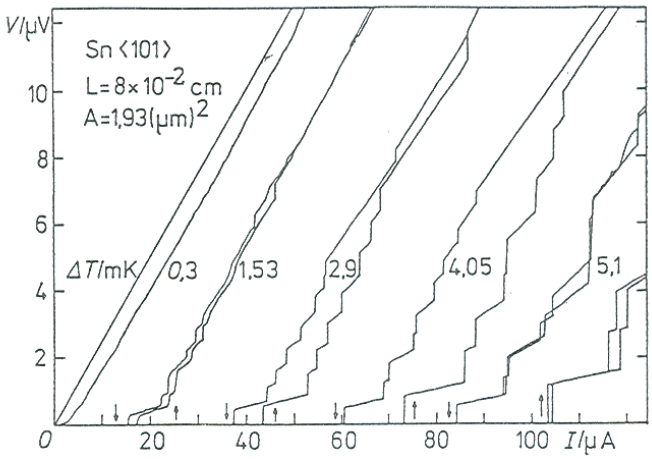

FIG. 1.2: Current-voltage (I-V) characteristic (increasing and decreasing current) of a Sn wire of radius $R = 0.78\mu$m at several fixed temperatures $T = T_{c0} - \triangle(T)$ (from Ref. [13]). A clear hysteresis is found with increasing and decreasing the applied current (indicated by arrows) with finite jumps in the I-V curve.

be effectively applied to study the stability of the normal state of the current-carrying superconductors and the mechanisms for a transition from this normal state to the superconducting state.

The behavior of superconductors in the presence of an electric field is far from the steady state and must be described by the dynamic equations of superconductivity. A comparative simple system of dynamic equations will be given below, which can also be derived from microscopic theory of superconductivity in a narrow temperature interval near the critical temperature for the superconducting transition, T_c [14, 15].

We denote by Δ and χ the modulus and the phase of the superconducting order parameter. We also introduce the gauge-invariant electromagnetic potentials $\mathbf{Q} = \mathbf{A} - (\hbar c/2e)\nabla\chi$ and $\Phi = \phi + (\hbar/2e)\partial\chi/\partial t$ where $\mathbf{A}$ and ϕ are the ordinary electromagnetic potentials. Requiring $D\kappa^2, \omega \ll \tau_{ph}^{-1}$, where D is the diffusion coefficient, τ_{ph} is the inelastic electron-phonon relaxation time, and κ and ω are the characteristic wave vector and frequency of the problem, the system of dynamic equations can be written in the following form [16]

$$-\frac{\pi}{8T}\sqrt{4\tau_{ph}^2\Delta^2+\hbar^2}\frac{\partial\Delta}{\partial t}+ \qquad \frac{\hbar\pi}{8T}D\nabla^2\Delta - \frac{\pi\hbar}{8T}D\left(\frac{2e}{\hbar c}\mathbf{Q}\right)^2\Delta$$
$$\frac{T_c-T}{T}\Delta - \frac{7\zeta(3)}{8\pi^2}\frac{\Delta^3}{T^2} = 0, \tag{1.1}$$

$$\frac{1}{\sqrt{4\tau_{ph}^2\Delta^2+\hbar^2}}\Delta^2\Phi + \frac{\Delta}{\hbar c}\mathrm{div}(\Delta^2\mathbf{Q}) = 0, \tag{1.2}$$

$$\mathbf{j} = \sigma\mathbf{A} - \frac{\sigma\phi\Delta^2}{2\hbar cT}\mathbf{Q}, \tag{1.3}$$

where

$$\mathbf{E} = -\frac{1}{c}\frac{\partial\mathbf{Q}}{\partial t} - \nabla\Phi. \tag{1.4}$$

In the gap free case, $\tau_{ph} \ll \hbar$, Eqs. (1.1)-(1.3) become the equations of the time-dependent Ginzburg-Landau theory. The relaxation of the potential Φ results from an interaction of the condensate with the excitations. In a gap free superconductor this interaction is strong, so that the electric field penetration depth is quite small, $l_E = (2DT\hbar/\pi\Delta^2)^{1/2}$, of the order of the coherence length $\xi(T)$, where

$$\xi(T) = \sqrt{\frac{\pi\Delta\hbar}{8(T_c-T)}}. \tag{1.5}$$

From Eqs. (1.1)-(1.3) we see that the characteristic frequency is of order

$$\omega_{GL} = \frac{\pi \Delta_{GL}^2}{2T\hbar}, \tag{1.6}$$

where

$$\Delta_{GL} = \sqrt{\frac{8\pi^2 T(T_c - T)}{7\zeta(3)}} \tag{1.7}$$

is the equilibrium value of the order parameter.

It is convenient to use Eqs. (1.1)-(1.3) in dimensionless units. In this case we adopt as the characteristic length and the characteristic time the quantities $\xi(T)$ and $\tau_{GL} = \omega_{GL}^{-1}$, respectively; the order parameter is divided by its equilibrium value Δ_{GL}; and its current is expressed in units of $\pi\sigma\Delta_{GL}^2/4eT\xi$. In terms of these units the critical Ginzburg-Landau current is $j_c = 2/3\sqrt{3} \simeq 0.385$. In dimensionless variables, our equations are

$$-u\left(\frac{\Delta^2}{\Gamma^2}+1\right)^{1/2}\frac{\partial\Delta}{\partial t} + \nabla^2\Delta + \left(1 - \Delta^2 - \mathbf{Q}^2\right)\Delta = 0, \tag{1.8}$$

$$u\Delta^2\left(\frac{\Delta^2}{\Gamma^2}+1\right)^{-1/2}\Phi + \mathrm{div}(\Delta^2\mathbf{Q}) = 0, \tag{1.9}$$

$$j = -\frac{\partial \mathbf{Q}}{\partial t} - \nabla\Phi - \Delta^2\mathbf{Q}, \tag{1.10}$$

$$\nabla^2\Phi - \mathrm{div}\frac{\partial\mathbf{Q}}{\partial t} = u\Delta^2\left(\frac{\Delta^2}{\Gamma^2}\right)^{-1/2}\Phi. \tag{1.11}$$

The gauge-invariant potentials in these units are $\Phi = \phi + \partial\chi/\partial t$, and $\mathbf{Q} = \mathbf{A} - \nabla\chi$. In Eqs. (1.8)-(1.11) we have introduced a depairing factor

$$\Gamma = \frac{\hbar}{2\tau_{ph}\Delta_{GL}} = \frac{\pi\hbar}{8\sqrt{u}}\frac{1}{\tau_{ph}T_c}\left(\frac{T_c - T}{T}\right)^{-1/2} \tag{1.12}$$

and the numerical parameter $u = \pi^2/14\zeta(3) \approx 5.79$.

The gap free situation corresponds to $\Delta \ll \Gamma$. The depairing factor Γ depends on temperature. In a narrow neighborhood of T_c the factor Γ is large, $\Gamma \gg 1$, so that we would always be dealing with gap-free situation. For those temperatures at which experiments are customarily carried out, however, the factor Γ is usually much less than unity. In such cases, therefore, when Δ is of the order of its equilibrium value, the inequality $\Delta \gg \Gamma$ usually holds. This inequality corresponds to the presence of a gap in the energy spectrum. In this situation, the electric-field penetration depth is given in order of magnitude by $l_E \sim (u\Gamma)^{-1/2}$, as can be seen from (1.11), and is much larger than $\xi(T)$.

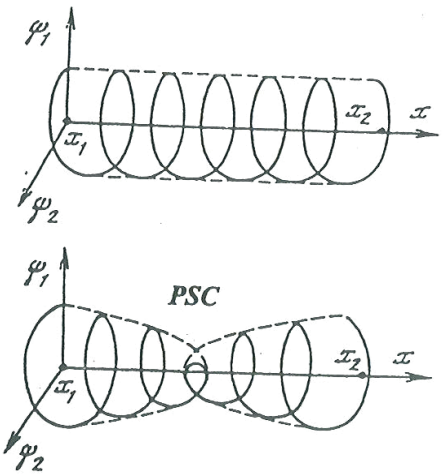

Fig. 1.3: Creation of phase-slip centers in a superconducting filament directed along the x-axis; ψ_1 and ψ_2 are real and imaginary parts of the superconducting order parameter.

1.1.2 Phase slip mechanisms

W. A. Little was one of the first who related the step structure of the I-V characteristics to the successive appearance of localized structures ("phase-slip centers") when he studied the stability problem of electric current in quasi-1D structures [17]. His idea about "phase slippage" was further developed in a number of works (see e.g. Refs. [7, 8, 12]).

To have an idea about phase slip process, let us consider two points, x_1 and x_2, of a superconducting filament (see Fig. 1.3) with potential $V(t)$. The time development of the phase difference of the superconducting order parameter $\varphi = \varphi(x_1) - \varphi(x_2)$ is given by the Josephson relation $\varphi = 2eV(t)/\hbar$ leading to

$$\varphi(t) = \varphi(0) + \frac{2e}{\hbar}\int_0^t V(t)dt, \tag{1.13}$$

where e is the electron mass. If the time average of the voltage is nonzero, but for instance $< V(t) >> 0$, the phase difference increases as a function of time. This leads to an increase of $\nabla\varphi(x)$ and thus to an increase of the superfluid velocity $v_s = (\hbar/m)\nabla\varphi(x)$ with m electron mass. As a consequence, the supercurrent density, which is given by $j_s = -(2e/m)|\psi|^2\hbar\nabla\varphi(x)$, increases. At the same time the absolute value of the order parameter decreases with increasing v_s [18]. On the other hand, the increase of $\nabla\varphi(x)$ beyond some critical value would lead to the inconsistency with a steady state. To avoid

this, a phase-loss mechanism is needed to reduce the phase difference. For this purpose 'phase-slip processes' are assumed to occur in the sample, each reducing the phase difference $\varphi(t)$ by 2π as it is shown in Fig. 1.3. A stationary state can be reached if in time average the phase difference generated by the voltage is destroyed by phase-slip processes. The period τ_{PSC} of the phase-slip process is given by

$$2\pi = \varphi(\tau_{PSC}) - \varphi(0) = \frac{2e}{\hbar}\int_0^{\tau_{PSC}} V(t)dt = \frac{2e}{\hbar} < V(t) > \tau_{PSC}. \qquad (1.14)$$

The repetition frequency of the phase-slip process is then

$$\omega_{PSC} = \frac{2e}{\hbar} < V(t) >, \qquad (1.15)$$

which is just the Josephson frequency [19].

1.1.2.1 The RSM Model Rieger, Scalapino, and Mercereau (RSM) [20] used TDGL equations to calculate the time behavior of the supercurrent density in a region of weakened superconductivity in a quasi-one-dimensional superconductor which is driven by an overcritical current. This overcritical current leads to an acceleration of the Cooper pairs, associated with an increase of the

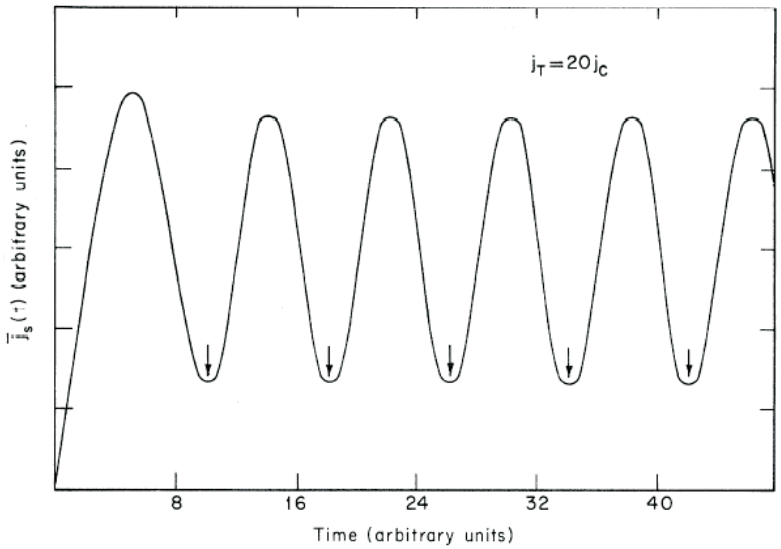

FIG. 1.4: Net supercurrent as a function of time in the phase-slip regime for the total current $j_T = 20j_c$ (j_c is the critical current). The arrows indicate the times of phase sip (from Ref. [20]).

supercurrent, and a decrease of the order parameter that decayed toward zero within a region of about one coherence length ξ. Soon the order parameter becomes very small and can be destroyed by fluctuations so that the phase-slip process can happen. RSM assumed that the superconductor remains in a phase-coherent state as long as the amplitude of the order parameter is nonzero and that the supercurrent in this case can be calculated by the time dependent GL theory. The phase-slippage is grafted onto the problem by assuming that the phase slip of -2π occurs instantaneously if the free energy of the region $\xi(T)$ becomes larger than the free energy related to an order parameter with a phase difference reduced by 2π.

Using numerical calculations RSM obtained the time dependent supercurrent density $j_s(t)$, spatially averaged over the entire region of weakened superconductivity. Their astonishing result is that $j_s(t)$ does not decay toward zero after the critical current j_c of the weak link is reached, but oscillates at a frequency which increases with increasing applied total current density j (see Fig. 1.4). The reason is that the order parameter grows again after the phase-slip event. The oscillation frequency of the supercurrent is found to be equal to the Josephson frequency as given in Eq. (1.15).

RSM pointed out that for depressed total current density, j, the part $j-j_s(t)$ has to be carried as 'normal' current so that the time averaged voltage across the weak superconductor is given by

$$< V(t) > (I) = R(I- < I_s(t) >). \tag{1.16}$$

Here, I and I_c are the total current and the supercurrent, respectively. RSM assumed the resistance R to be equal to the normal residual resistance of the weakly superconducting region. The relation between the total current and the phase of the order parameter is given by

$$I_c = (1/2)I_c(1 + \cos\varphi_{12}(t)), \tag{1.17}$$

where $\varphi(t)$ as given by Eq. (1.13) with $V(t) = R(I - \overline{I}_s(t))$ is the phase difference across the weak link. For $I_c \gg I$ the current-phase relation predicts a nearly sinusoidal time dependence of the supercurrent. For $I \approx I_c$ the time dependence of the supercurrent is nonsinusoidal.

The knowledge of the current-phase relation is essential for the description of the superconducting properties. Therefore, $I_s(\varphi)$ has been measured for several weak-link structures [21, 22]. These measurements show that $I_s(\varphi)$ is nearly sinusoidal for point contacts and short microbridges but may strongly deviate from a sinusoidal to a nonsinusoidal behavior of $I_s(\varphi)$ with increasing length of the weak link as expected from theory [23].

1.1.2.2 The SBT Model In their model, Skocpol, Beasley and Tinkham (SBT) [12] explicitly neglect deviations from electrical neutrality, so they have $j_n+j_s = j$. The time evolution of j_s depends on the behavior of the electrochemical potential μ_p during the phase-slip cycle. The time average $< \mu_p >$ is assumed

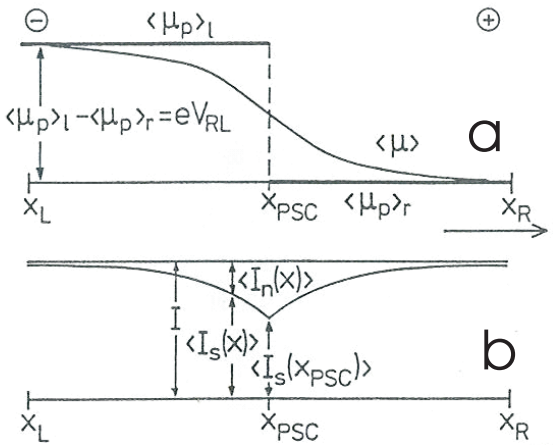

FIG. 1.5: Characteristic features of the SBT model of a phase-slip center (a) Time averaged electrochemical potentials of the Cooper pairs $< \mu_p >$, and the quasiparticles $< \mu >$. Furthermore, x_L and x_R are two points far away from the phase-slip center,, where $\mu = \mu_p$. Here, $\ominus$ and $\oplus$ indicate the polarity of the battery. (b) Behavior of the time averaged supercurrent and 'normal' current at different points (from Ref. [12]).

to be constant in space with a step-like change at x_{psc} They assumed that variations of the order parameter occur on the length scale of -2Λ, where Λ is the quasiparticle diffusion length, essentially a quasiparticle mean free path. The order parameter is assumed to be identically zero only at the center of the PSC. The characteristic features of the SBT model [18, 24] are sketched in Fig. 1.5. SBT assumed that all of the applied voltage gets dropped right at the core of PSC, so that in their steady state approximation, there is no variation in the time-averaged value $< \mu_p >$ inside the superconducting regions. However $< \mu_p >$ experience sharp steps at each PSC. Of course, the actual μ_p will vary, corresponding to the variations of the superconducting phase, as given by the Josephson relation $\mu_p = -\frac{\hbar}{2}\frac{\partial \phi}{\partial t}$.

Since the voltage is only dropped at the core of the PSC, it is a reasonable approximation to take

$$eV = \triangle\mu, \tag{1.18}$$

i.e.

$$V = \frac{\triangle\mu}{e} \approx 2\rho\Lambda(j - j_s) = \frac{2\rho\Lambda}{\sigma}(I - I_s)_{x>x_{psc}}, \tag{1.19}$$

with σ the conductivity in the normal state and $e = |e|$, the absolute value of the electronic charge. Notice that since the voltage drop is due to the normal current only, the above relation uses μ rather than μ_p.

Based on the expected shape of μ_p during the first half of the cycle (*i.e.* when the supercurrent gets accelerated), SBT modelled it as:

$$\mu_p = \frac{\mu_p}{2}(1 - \tanh(\frac{x - x_{psc}}{\pi\xi})) + < \mu_p >, \tag{1.20}$$

The μ_p for the deceleration part is assumed to be close to the asymptotic values away from the PSC, but with a gradient which is $-\gamma$ times that of the above expression and is discontinuous at $x = x_{psc}$. Here the parameter γ specifies the relative times for the acceleration and deceleration parts of the cycle. SBT used $\gamma \gg 1$, which corresponds to an instantaneous deceleration, a 'snap back' of the phase.

SBT further used the Pippard, Shepherd and Tindall result [25]: $< \mu > - < \mu_p >= \Lambda^2 \frac{d^2}{dx^2}(< \mu > - < \mu_p >)$. They solved this equation on both sides of the PSC, such that on both sides they assumed the presence of bulk regions (say at x_l and x_r), where $< \mu >=< \mu_p >$. They then have, say on the left side of the PSC:

$$< \mu > - < \mu_p >= U \sinh(\frac{x - x_l}{\Lambda}). \tag{1.21}$$

Now, assuming $x_l \gg \Lambda$ and $x_r \gg \Lambda$:

$$\begin{aligned} V = \frac{\triangle\mu}{e} = \rho\Lambda(\tanh(\frac{x_{psc} - x_r}{\Lambda}) - \tanh(\frac{x_l - x_{psc}}{\Lambda}))(j - < j_s >) \\ \approx 2\rho\Lambda(j - < j_s >). \end{aligned} \tag{1.22}$$

Then

$$\frac{dV}{dj} \approx 2\rho\Lambda. \tag{1.23}$$

This then suggests that each PSC contributes a differential resistance of $\frac{2\rho\Lambda}{\sigma}$. Since each phase-slip center can carry about $0.6I_c$, it follows that the experiments should show this excess current. Furthermore, as more and more PSCs develop, the dissipative processes should contribute to larger and larger differential resistance, so that the I-V curve is predicted to have step-like nature, with each step being a straight line with a $\sim 0.6I_c$ zero voltage intercept.

Several groups also conducted experiments where $< \mu >$ and $< \mu_p >$ were directly measured. Dolan and Jackle [26] measured both $< \mu >$ and $< \mu_p >$ in long microbridges of tin and indium, using opposed sets of normal and superconducting probes with oxide barrier tunnel junctions, and showed that indeed $< \mu >$ varies smoothly, while $< \mu_p >$ varies abruptly at the PSC. Other similar experiments were carried out by Aponte and Tinkham [27] and Stuivinga et al. [28].

1.1.3 Application of the Ginzburg-Landau theory

Although derived in a close vicinity of the critical temperature T_c the TDGL theory have being successfully used to study the nonequilibrium processes in

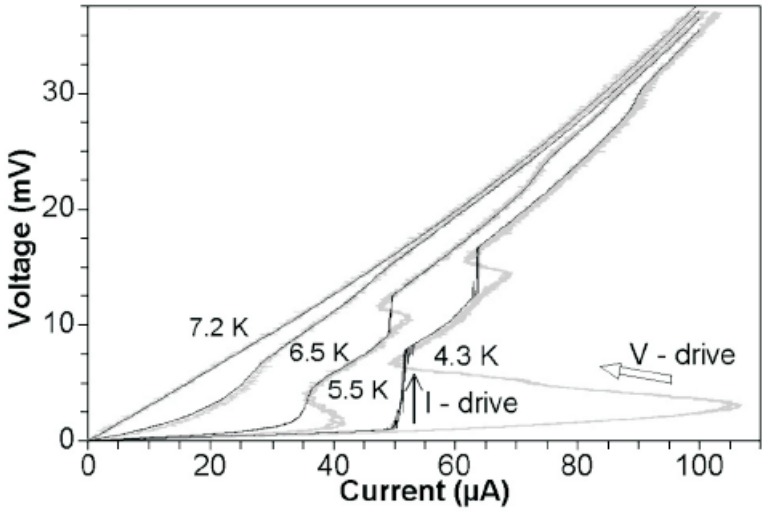

FIG. 1.6: I-V characteristics of a Pb nanowire (radius 20 nm, length 22 μm) at different temperatures. Results are shown for the current driven mode (black curves) and the voltage driven mode (grey curves) (from Ref. [32]).

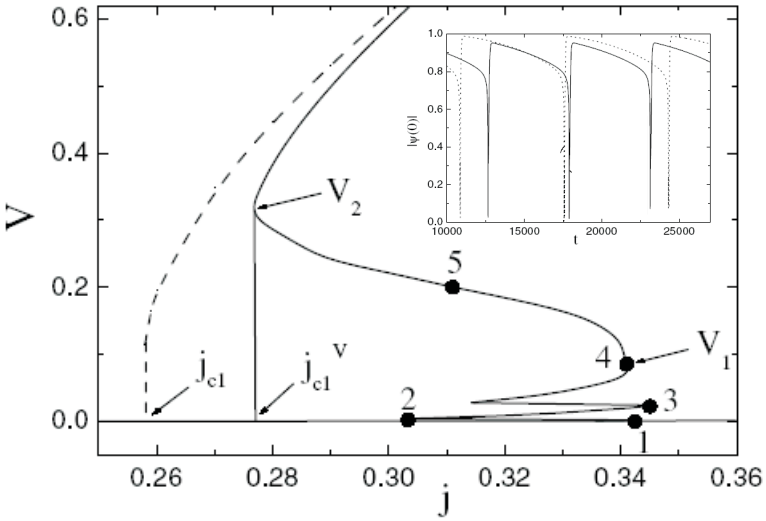

FIG. 1.7: The current-voltage characteristics of a superconducting wire of length 40ξ and $\gamma = 10$. Dashed (solid) curve for current (voltage) constant regime. The inset shows the time dependence of the order parameter in the center of the wire. The solid (dotted) curve corresponds to the voltage in point 1 (2) in the main panel (from Ref. [32]).

current carrying superconducting samples [29–36]. The experiments in superconducting Pb nanowires in the voltage constant regime has shown an unexpected S-shape response (see the grey curves in Fig. 1.6), while no such behavior is obtained in the constant current regime (black curves in Fig. 1.6). Instead usual finite voltage jumps are see in the latter case. Such S-shape behavior is also obtained within the TDGL theory (see Fig. 1.7) and it was shown that such unusual behavior is a direct consequence of the dynamics of the superconducting condensate and of the existence of two different critical currents: j_{c2} at which the pure superconducting state becomes unstable and $j_{c1} < j_{c2}$ at which the phase slip state is realized in the system. A simple model was established [33] which gives the condition of the appearance of periodic in time (see the inset of Fig. 1.7) in such 1D samples. The TDGL theory was successfully used to describe negative resistance in superconducting nanowires [35] and to study the effect of acdriven phase slip centers [29].

Very recently, Rubinstein et al. presented a simple explanation to the PSC phenomenon in a 1D wire using TDGL model. Retaining temperature and applied current as parameters, they established where in this parametric space these oscillatory solutions can be found. One of the most interesting features of the analysis was the evident collision of real eigenvalues of the associated PT-symmetric linearization, leading to the emergence of complex elements of the spectrum.

1.2 SUPERCONDUCTING FILMS: FLUX FLOW INSTABILITY AND FORMATION OF PHASE SLIP LINES

When a thin superconducting film is placed in a perpendicular magnetic field that is larger than some critical value H_c, Abrikosov vortices penetrate the sample and form a triangular vortex lattice in the absence of pinning [37]. If now a transport current is applied to the sample vortices start moving under the action of the Lorentz force of the current. The vortex motion leads to energy dissipation in the system and to a finite voltage and electrical field in the superconductor. At large vortex line velocities, the vortex motion becomes unstable and a nonequilibrium distribution of the quasiparticles appear, which leads to an electronic instability and an abrupt switching into a state with higher electrical resistivity, i.e., the voltage-current characteristic exhibits a hysteretic jump, as predicted by Larkin and Ovchinnikov (LO) [38]. Namely, when the vortex moves with a velocity v, the order parameter ψ in the vortex core varies on a time scale $\tau_{|\psi|} \sim \xi/v$ that can be smaller than the relaxation time of the nonequilibrium quasiparticles τ_{in} (due to inelastic electron-phonon or electron-electron interactions). As a consequence, the quasiparticle distribution function deviates from its equilibrium and it results to a shrinkage of the vortex core at temperatures close to the critical one [38]. This effect is

mainly connected with the removal of quasiparticles from the vortex core by the induced electric field [39] and, in some respect, is similar to the dynamic enhancement of superconductivity in weak superconducting links [18, 39].

Electric-field induced flux flow instabilities intensively studied in the past both in low [39–42] and high [43–47] temperature superconductors, in general agree reasonably well with the LO theory. However, in some cases, the LO theory turns out to be insufficient to describe the experimental results. For example, at low temperatures the LO description breaks down, suggesting a different origin for the flux flow instabilities [41]. Explanation for the flux flow instabilities beyond the original or modified LO picture were sought in dynamic vortex lattice crystallization [48], depinning phenomena [49], apperance of hot spots [50], and recently in vortex core expansion due to electron heating at low temperatures [51].

However, in the original LO theory the question about vortex structure before and after the transition was not considered. At the end of the 70s it was speculated that lines with fast vortex motion (so called phase slip lines) should appear in the superconductor at the transition point. Because analytical calculations are strongly restricted due to the mathematical complexity of the problem, only a semi-quantitative analysis was made using the assumption that phase slip lines already exist in the sample [52].

A number of works have been published were vortex motion was studied theoretically using a numerical simulation of the extended time-dependent Ginzburg-Landau (GL) equations [53–56] where the time τ_{in} of the nonequilibrium quasiparticle distribution function was explicitly included. In Refs. [53, 54] two types of vortex motion were found: slow and fast vortex motion (the latter was named the kinematic vortex [54]). However, neither the influence of the magnetic field nor the transition between these types of motion nor the transformation of the vortex lattice were addressed. In Ref. [55] the deformation of the vortex core due to the finite relaxation time of the order parameter was found and a short range attraction between vortices was predicted.

To answer the question of what happens with the vortex structure when the critical velocity is reached, one should use a rather complicated set of integro-differential equation for the order parameter, Green's functions of the superconductor, and quasiparticle distribution function [38]. It is very difficult to solve these equations even numerically. Therefore, in a recent paper [56] the rearrangement of the vortex lattice due to the above effect and the transition from the slow to the fast vortex motion (phase slip line) were studied for an infinitely long superconducting slab placed in a parallel magnetic field using the extended time-dependent Ginzburg-Landau equations. It was shown that, with increasing the applied current, the moving vortex lattice changes its structure from a triangular one to set of parallel vortex rows in a pinning free superconductor (see Fig. 1.8). This effect originates from the change of the shape of the vortex core due to nonequilibrium effects. The moving vortex creates a

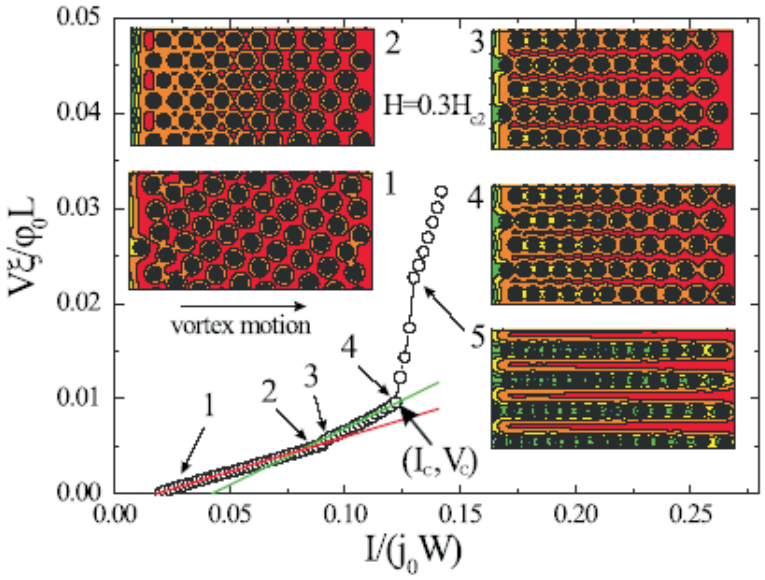

Fig. 1.8: Current-voltage characteristics of the superconducting slab with width $W = 50\xi$, $\gamma = 10$, and $H = 0.3H_{c2}$. The system has a periodic boundary in x-direction and uniform current, flowing in y-direction, increases from zero to some finite value. Insets show the transition of the triangular arrangement of vortices (inset 1) to the row of moving vortices (inset 3) and later to the vortex channels (or phase-slip lines) (inset 5). These transitions correspond to the jumps in the I-V curve, indicated by the numbers. (from Ref. [56]).

defect of quasiparticles in front of its motion and an excess of quasiparticles behind the core of the moving vortex. This results in the appearance of weak (regions with suppressed order parameter) behind the vortex, which attracts other vortices resulting in a effective direction dependent interaction between vortices. When the vortex velocity reaches the critical value, phase slip lines appear, which may coexist with slow moving vortices between such lines.

In most of the experiments devoted to the study of transport properties of superconducting samples, a microbridge geometry is used in order to reduce the power dissipation in the system. However, in the presence of an external magnetic field the bulk superconducting leads may turn into a normal state while the microbridge is still superconducting, which considerably changes the experimental picture. Thus, in most of the cases we have to deal with normal contacts. The presence of normal electrodes is in general closer to the real experimental situation, which may change the properties of the whole system in comparison with the solitary mesoscopic origin due to also possible quantum

interference. Therefore, a problem of how the normal contacts and the finite size of the sample influences to the dynamics of vortices needs to be solved.

1.3 DETAILS OF THE NUMERICAL APPROACH

Equations (1.8)-(1.10) can also be written in complex form by introducing the complex order parameter $\psi = \Delta \exp i\chi$:

$$\frac{u}{\sqrt{1+\gamma^2|\psi|^2}}\left(\frac{\partial}{\partial t} + i\varphi + \frac{\gamma^2}{2}\frac{\partial|\psi|^2}{\partial t}\right)\psi = (\nabla - i\mathbf{A})^2\psi + \left(1 - T - |\psi|^2\right)\psi, \tag{1.24}$$

$$j = -\nabla\varphi - \frac{\partial \mathbf{A}}{\partial t} + \frac{1}{2i}\left(\psi * \nabla\psi - \psi\nabla\psi*\right) - |\psi|^2\mathbf{A} = \kappa^2\nabla\times\nabla\times\mathbf{A}, \tag{1.25}$$

where $\gamma = 1/\Gamma$, φ is the electrostatic potential, and $\kappa = \lambda/\xi$ is the Ginzburg-Landau parameter, with λ-magnetic field penetration depth and ξ-the coherence length. As we consider only extreme time-II superconductors, i.e. $\kappa \gg 1$, the demagnetization effects can be neglected and instead of solving Eqs. (1.24) and (1.25), we solved only the first GL equation (1.24), supplemented with the equation for the electrostatic potential

$$\nabla^2\varphi = \mathrm{div}\left(\mathrm{Im}\left[\psi * (\nabla - i\mathbf{A})\,\psi\right]\right). \tag{1.26}$$

The latter is nothing else than the condition for the conservation of the total current in the sample, i.e. div$\mathbf{j} = 0$. In Eqs. (1.24) and (1.26) all the physical quantities are measured in dimensionless units: temperature in units of the critical temperature T_c, the vector potential $\mathbf{A}$ and the momentum of the superconducting condensate $\mathbf{p} = \nabla\phi - \mathbf{A}$ are scaled in units of $\Phi_0/[2\pi\xi(0)]$ (where Φ_0 is the quantum of magnetic flux), the order parameter in units of Δ_0 and the coordinates are in units of the coherence length $\xi(0) = (8k_BT_c/\pi\hbar D)^{-1/2}$. In these units the magntic field is scaled with $H_{c2} = \Phi_0/2\pi\xi(0)^2$ and the current density with $j_0 = \sigma_n\hbar/2e\tau_{GL}(0)\xi(0)$. Time is scaled in units of the GL relaxation time $\tau_{GL}(0) = \pi\hbar/8k_BT_cu$, the electrostatic potential φ is in units of $\varphi_0 = \hbar/2e\tau_{GL}(0)$ (σ is the normal state conductivity and D is the diffusion constant). We put $\mathbf{A} = (Hx, 0, 0)$ because we limit ourselves to the case when the effect of the self induced magnetic field is negligible.

A superconductor-insulator boundary condition $(-i\nabla - A)\psi|_{\mathbf{n}} = 0$ is used for the order parameter and the Neumann boundary condition $\nabla\varphi|_{\mathbf{n}} = 0$ is applied for the electrostatic potential with $\mathbf{n}$-the unit vector normal to the surface of the superconductor. In order to inject the current into system we

used normal metal-superconductor boundary conditions at the contacts, i.e. $\psi = 0$ and $\nabla\varphi = j_{ext}$. In the case of bridge geometry, "bridge" boundary conditions: $|\psi(0)| = |\psi(L)| = 1$, $\psi(0, t + dt) = \psi(0, t)e^{-i\varphi(0)dt}$, $\psi(L, t + dt) = \psi(L, t)e^{-i\varphi(L)dt}$, and $\varphi(0, t) = 0$ (L is the sample length) are used.

For fixed applied magnetic field, we solved the Eqs. (1.24) and (1.26) self-consistently introducing the complex link variables [57]

$$U_{x,y}^{r_1,r_2} = \exp \int_{r_1}^{r_2} \mathbf{A}_{x,y}(\mathbf{r})\mathrm{d}x, y. \tag{1.27}$$

These link variables are used in order to preserve the gauge-invariance of discretized GL equations. A finite-difference representation of the order parameter, vector potential and electrostatic potential is given on a uniform cartesian space grid (x,y) with typical grid spacing smaller than 0.5ξ. We used implicit iterative Euler method to solve the Eq. (1.24) and Fourier transform method for the solution of the Eq. (1.26) for the electrostatic potential.

2

Critical currents of the phase-slip process in the presence of electromagnetic radiation, Rectification for time asymmetric ac signal

2.1 INTRODUCTION

At the present moment there are several well-known phenomena connected with the interaction of electromagnetic (e.m.) radiation with superconductors. These are the destruction of superconductivity by e.m. radiation with frequency $\nu > 2\Delta/\hbar$ (Δ is the superconducting gap), simulation of superconductivity [58] (Eliashgberg effect) by e. m. radiation with frequency $\nu \ll 2\Delta/\hbar$, and appearance of Shapiro steps in the current-voltage characteristics of Josephson junctions [59]. Recently, Shapiro steps were also observed in superconducting strips in the absence of Josephson junctions [60]. These Shapiro steps were explained by the existence of phase-slip lines [16, 18, 61] in the sample and their interaction with external e. m. radiation [60].

We investigated the effect of *e.m.* radiation on the critical current of the phase-slip process in a regime when there is no stimulation superconductivity. Surprisingly, practically no theoretical studies exist on this subject. We found that at large enough power of the ac signal in the superconductor oscillations appear in the critical currents similar to what has been observed in Josephson junctions [62]. We will also show that if the applied signal is asymmetric in time, it may lead to a ratchet effect as was shown in recent experiments Ref. [63] on annular Josephson junctions.

We introduce the model and set of equations which are numerically solved. A and B for the cases of time symmetrical and asymmetrical ac signals, respectively. We compare our results with the well-developed theory of Josephson junctions and discuss the experimental conditions under which they may be observed experimentally.

2.2 THEORETICAL MODEL

For our theoretical study we use the generalized time-dependent Ginzburg-Landau (TDGL) equations

$$\frac{u}{\sqrt{1+\gamma^2|\psi|^2}}(\frac{\partial}{\partial t}+i\varphi+\frac{\gamma^2}{2}\frac{\partial|\psi|^2}{\partial t})\psi=\frac{\partial^2\psi}{\partial x^2}+(1-T-|\psi|^2)\psi, \tag{2.1}$$

$$j=Im(\psi^*\nabla\psi)-\frac{\partial\varphi}{\partial x} \tag{2.2}$$

with explicit inclusion of time relaxation τ_ϵ (through the coefficient $\gamma=2\tau_\epsilon\Delta_0/\hbar$) for the nonequilibrium quasiparticle distribution due to the electron-phonon interaction [14, 15] and $\triangle_0=4\kappa_BT_c/u^{1/2}$ is the 'effective' value of the order parameter at T=0. In Eqs. (2.1) all the physical quantities (order parameter $\psi=|\psi|e^{i\phi}$, electrostatical potential φ) are measured in dimensionless units: the momentum of the superconducting condensate $p=\nabla\phi$ is scaled by the unit $\Phi_0/[2\pi\xi(0)]$ (where Φ_0 is the quantum of magnetic flux), the order parameter is in units of Δ_0 and the coordinates are in units of the coherence length $\xi(0)=(8\kappa_BT_c/\pi\hbar D)^{-1/2}$ (D is the diffusion constant). In these units the current density is scaled with $j_0=\sigma_n\hbar/2e\tau_{GL}(0)\xi(0)$, time is in units of the Ginzburg-Landau relaxation time $\tau_{GL}(0)=\pi\hbar/8\kappa_BT_cu$ and the electrostatic potential φ is in units of $\varphi_0=\hbar/2e\tau_{GL}(0)$ (σ_n is the normal-metal conductivity). The vector potential is equal to zero because there is no magnetic field and self-induced effects are small for our system.

Strictly speaking, the validity of Eqs, (2.1) was demonstrated theoretically only near the critical temperature $T-T_c<\hbar/(\kappa_B\tau_\epsilon)$ and for frequencies $\upsilon<1/\tau_\epsilon$. Using the value $\tau_\epsilon(T=T_c)\sim 3X3^{-10}s$ and $T_c\sim 3.8K$ which are typical for tin, we find that for this material Eqs. (1) should give reasonable results for $\upsilon<3GHz$ and $T_c-T<0.002K$. From previous applications of the TDGL equations we expect that our results may be applicable, at least qualitatively, for higher frequencies and even from T_c. We use a one-dimensional model assuming that in the considered temperature range the width of the film satisfies $W<\lambda^2/d$ with thickness $d<\lambda$ and hence the current density distribution is practically uniform over the film width. In our calculations we used $T=T_0=0.9T_c$ and two values for the parameter $\gamma=40,120$ (for tin $\gamma\sim 160$ and for lead $\gamma\sim 21$). It is more convenient to express the different

quantities in units normalized at $T = T_0$. So, for example, with j_0 we mean $j_0(T = 0.9T_c) = 0.1^{3/2} j_0(T = 0)$ and with $\tau_{GL}(T = 0.9T_c) = 10\tau_{GL}(T = 0)$. The length of the sample was taken equal to $L = 20\xi(T = 0.9)$ which is larger than the penetration depth of the electric field for used values of γ and temperature.

To simulate a real experimental situation we use "bridge" boundary conditions $|\psi(-L/2)| = |\psi(L/2)| = 1$, $\psi(\pm L/2, t+dt) = \psi(\pm L/2, t) \exp^{-i\varphi(\psi(\pm L/2)dt)}$, and $\varphi(-L/2, t) = 0$. The Euler method is used to solve Eqs. (2.1) and (2.2). Initial conditions were $|\psi| = 1$ and $\varphi = 0$ at moment $t = 0$. A phase-slip center appears (at some critical current) always in the center of the wire, because there the order parameter is minimal due to the chosen boundary conditions. Because of the relatively small length L, only one phase-slip enter nucleates. With increasing L the number of phase-slip centers increases and the dynamic of the system very complicated, and therefore this case is not considered.

In the experiment the induced currents are distributed uniformly over the sample because the wavelength of the applied electromagnetic radiation is usually much larger than the sample size. Therefore, in our theoretical model we may assume that the full current in the film is $j = j^{dc} + j^{ac} \sin(2\pi\upsilon t)$, with υ the frequency of the applied e.m. radiation. In order to include heating effects we also solved the equation for the temperature distribution in the sample.

$$C_{eff} = \frac{\partial T}{\partial t} = K_{eff} \triangle T + j_n^2 - h(T - T_0), \tag{2.3}$$

where $C_{eff} = (D_s C_s/d_f + C_f) T_c \sigma_n / \tau_{GL}(0) j_0^2$, $K_{eff} = (D_s k_s/d_f + k_f) T_c \sigma_n / \xi^2 j_0^2$, $h = k_s T_c \sigma_n / D_c d_f j_0^2$, the heat transfer coefficient h governs the heat removal from the sample, and C_s, C_f, k_s, and k_f are heat capacity and heat conductivity of the substrate (subscript s) and film and sample (subscript f), respectively. Here we used a model for the temperature distribution in thin superconducting films as was previously discussed in details in Ref. [64] and we assumed that the thickness of the substrate and film, $D_s + d_f$, is much smaller than the heating length $\Lambda_h = \sqrt{K_{eff}/h} > D_s + d_f$. If $D_s C_s/d_f \ll C_f$ and $D_s k_s/d_f \ll k_f$, we can use the Wiedermann-Franz law as an estimate for C_f and k_f and we obtain $C_{eff} = \pi^3/48 \simeq 0.65$ and $K_{eff} = \pi^4/48u^2 \simeq 0.06$ at temperature close to T_c. Because of the uncertainly in the actual value of k_s, we use h as a parameter to distinguish the cases of complete heat removal ($h = 10^{-1}$) and weak heat removal ($h = 10^{-4}$).

2.3 NUMERICAL RESULTS

2.3.1 A) Symmetric ac signal

As is well known, the phase-slip process is usually hysteretic (see the review in Ref. [65] and the books in Refs. [18] and [61]. There are two critical currents:

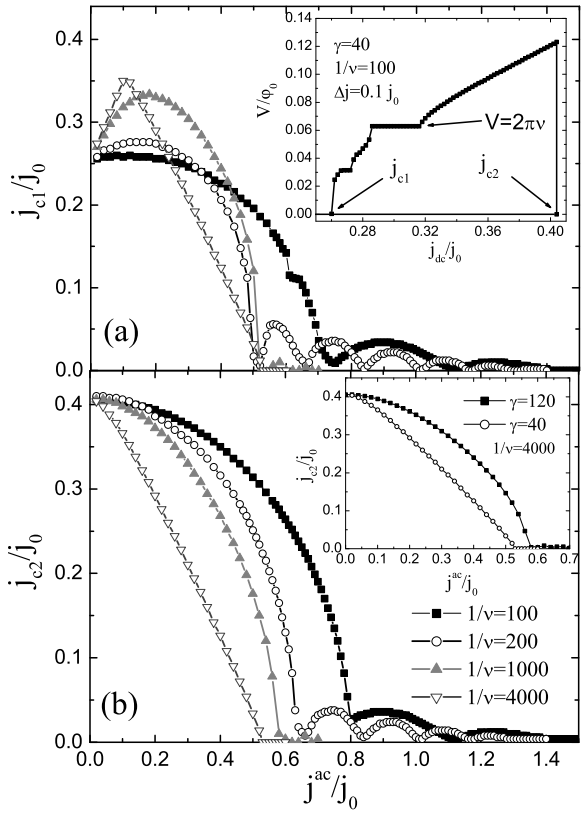

Fig. 2.1: Dependence of (a) j_{c1} and (b) j_{c2} on the amplitude of the ac signal for different values of the period $1/\nu$ of the e.m radiation. $\gamma = 40$ and heat coefficient h=0.1. In the of (a) we show typical current-voltage characteristics of the superconductor for a small period of the e;m; radiation. The inset of (b) shows the dependence of $j_{c2}(j^{ac})$ on the parameter γ.

j_{c1}, which characterized that for $j < j_{c1}$ the phase-slip process vanishes in the superconductor, and j_{c2}, at which the superconducting resistiveless state becomes unstable (in a defectless sample j_{c2} is equal to the depairing current density). In Ref. [32] it was argued that the first critical current is connected to the competition of two process: the growth of the magnitude of the order parameter and the growth the momentum p in the phase-slip center (PSC). If the order parameter grows faster than the momentum, the phase-slip process

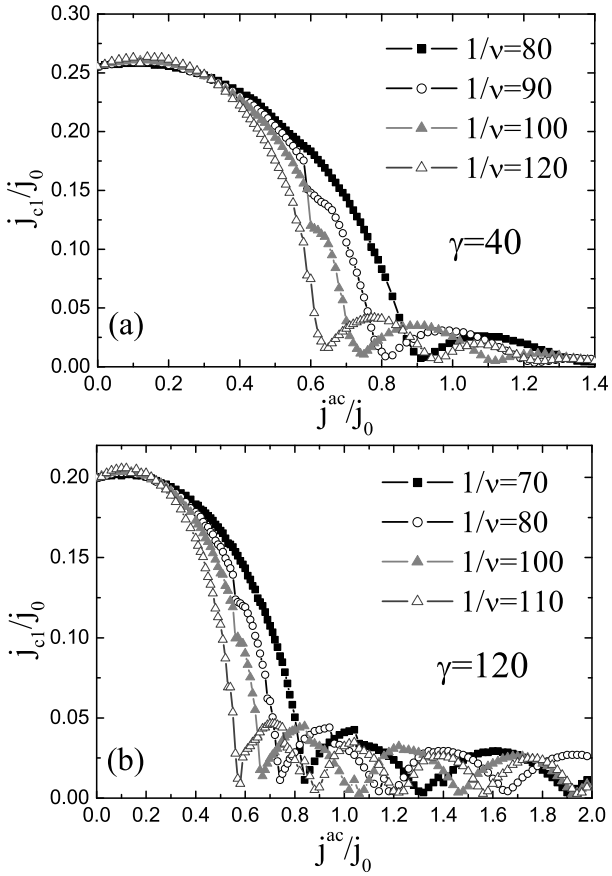

FIG. 2.2: Dependence of j_{c1} [for two values of the parameter γ. (a) $\gamma = 40$ and $\gamma = 120$] in the range of e.m. radiation where oscillations in j_{c1} are most pronounced.

cannot occur in the sample. A finite relaxation time for the magnitude of the order parameter τ_ψ results in a voltage jump ΔV at the current $j = j_{c1}$ [32].

In this section we study how the ac component of the current affects the value of $j_{c1}(j^{ac}, \upsilon)$ and $j_{c2}(j^{ac}, \upsilon)$. In this respect the above-mentioned currents j_{c1} and j_{c2} may be considered as a particular case of zero ac current $j^{ac} = 0$ and we will use the notation $j_{c2}(0)$ and $j_{c1}(0)$ for that case. In Fig. 2.1 we present the dependencies of j_{c1} and j_{c2} for different values of the period $1/\upsilon$ of the radiation, with $\gamma = 40$ and for almost perfect heat removal [h=0.1 in Eq.2.3].

The main features of such a behavior may be explained by the finite relaxation time of the magnitude of the order parameter $\tau_{|\psi|}$. If built on an analogy with Josephson junctions, this time provides for the superconductor some kind of "inertia" term.

First we discuss j_{c2}. At large enough period of the e.m. radiation $1/\upsilon$, the order parameter has sufficient time to adopt itself to any change of the external current. When the sum $j^{dc} + j^{ac}$ becomes larger than $j_{c2}(0)$, phase slips appear in the sample and $j_{c2} = j_{c2}(0) - j_{ac}$ changes linearly with j^{ac}. With increasing frequency of the radiation it is necessary to increase the sum $j^{dc} + j^{ac}$ above $j_{c2}(0)$ because of the finite relaxation time of $|\psi|$. The smaller period $1/\upsilon$, the larger this increase of the sum has to be, and it results in a nonlinear dependence of j_{c2} on j_{ac} at high frequencies.

This result gives us the possibility to determine experimentally the relaxation time ($\tau_{|\psi|}$) by applying e.m. radiation with different frequencies and measuring its $j_{c2}(j^{ac})$ dependence. For example, for the parameters used in Fig.2.1 deviation of j_{c2} from a linear behavior starts at $1/\upsilon \lesssim 4000$. From this we may conclude that the order parameter decays from its equilibrium value to zero in about $4000\tau_{GL}(T = 0.9)$ (at the considered values of γ) if we apply to the sample a dc current which slightly exceeds j_{c2}. This method allows us to obtain a rough estimate, because this time depends strongly on the value of the dc current (See Refs. [18] and [66]).

A similar reasoning can be utilized to explain the behavior of $j_{c1}(j^{ac})$. At low frequencies, j_{c1} at first increases because the difference $j - j^{ac}$ may become less than $j_{c1}(j^{ac} = 0)$ at some moment in time and hence the phase-slip process will decay and cannot occur if $j^{dc}+j^{ac} < j_{c2}(0)$. For $j^{ac} < [j_{c2}(0)-j_{c1}(0)]/2$ the j_{c1} increases linearly with j^{ac}. When $j^{ac} = [j_{c2}(0) - j_{c1}(0)]/2$ the hysteresis in the current-voltage characteristic disappears, $j_{c1} = j_{c2}$, and we recover the scenario as described above. For high frequencies the finite relaxation time of the magnitude of the order parameter starts to play an essential role. It smooths the dependence of j_{c1} and removes the maximum at low amplitudes. Concurrently, the hysteresis in the I-V characteristics persists up to much higher values of j^{ac}. The reason is that the order parameter cannot vary substantially during a short time and hence it simply does not notice small oscillations of the ac current.

Another feature becomes visible when we got to higher frequencies: an oscillating dependence of j_{c1} for large amplitudes j^{ac} (see Figs.2.1 and 2.2). Actually these oscillations are also present at low frequencies but their amplitude and period are very small. The origin of these ocsillations is following. When the amplitude of the ac current becomes sufficiently large (the larger period, the smaller the amplitude, but definitely larger than j_{c2}) phase-slips are created in the system even for j^{dc}. However, it does not lead to a nonzero voltage because of the symmetry of the ac signal. The number of phase-slip events is the same for positive and negative currents. The smaller the period $1/\upsilon$, the smaller the number of events at constant j^{ac}. For example, at $1/\upsilon = 200$we have one

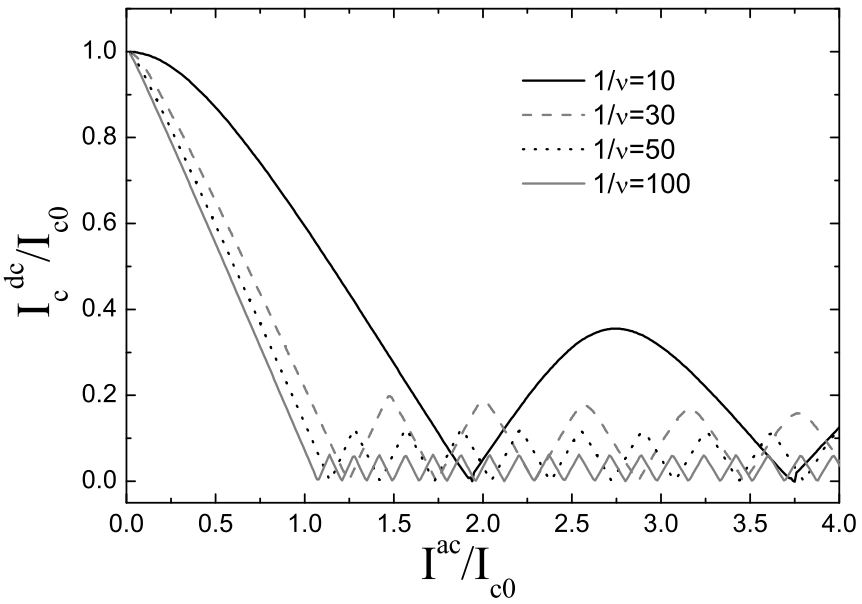

FIG. 2.3: Dependence of the dc critical current on the amplitude of the ac current in a Josepshon junction within the RCSJ model for a damping parameter $\beta_c = 0.01$ (see Ref. [18]). Current is measured in units of the Josepshon critical current I_{c0}, and time is in units $\tau_J = 2eI_{c0}R/\hbar$ where R is the resistance of the junction in the normal state.

"negative" (leading to negative voltage) and one "positive" (leading to positive voltage) PS event at the first oscillation of j_{c1} [at $0.58 < j^{ac} < 0.68$ in Fig. 2.1(a)], two "positive" and two "negative" for the second one, and so on. For larger period we have already many PS events during the first oscillation.

When we add positive dc current to the original ac current, we increase the time during which the current is positive and it raises the number of positive phase-slip events. But there is some kind of "resistance" which wants to preserve the number of PS events. The origin of this resistance is the finite time needed for each PS event. The larger the amplitude of the ac current or the value of the dc current, the less time it takes for the system to create phase slips events can occur within a period [67]. The "weakest" points in the system where it is easy to "insert" an extra PS event are these points which are responsible for the change from the regime of two PS events to four, six,

and so on. In these points the current $j_{c1} \simeq 0$ [for $1/v = 200$ it occurs at $j^{ac} 0.52, 0.68, 0.84, ... - see Fig. 2.1(a)$]. The most "resistive" points correspond to the middle of every such an oscillation, and the current j_{c1} is maximal there. The interplay between these factors is the reason [68] for the decreasing amplitude and period of the oscillations in j_{c1} with increasing period $1/v$.

At high frequencies a discontinuity in j_{c1} is found (most pronounced for $1/v = 100$ in Fig. 2.2). Our calculations show that this occurs when the superconductor transits to zero-resistance (V=0) state from Shapiro step. We connect it with the existence of the commensurablility between the intrinsic frequency which "helps" to keep the phase-slip process even at small enough dc current in the presence of radiation. This explains why the effect only for $v \gtrsim 1/\triangle V$ ($\triangle V$ is the value of the jump of the voltage $j = j_{c1}$ in absence of e.m. radiation) because $1/\triangle\triangle V$ is the minimal possible intrinsic frequency of the phase-slip process [68]. We should note that these jumps, also exist in the region where j_{c1} oscillates with increasing amplitude j^{ac}.

It is instructive to compare our results with the well-developed theory of Josephson junctions (see, e.g., Ref. [62]). The phase-slippage process in Josephson (tunnel or weak link) junctions resembles the phase-slip centers found in uniform superconducting films. The phase changes 2π after each phase-slip event in both systems. The main difference is that the order parameter is strongly suppressed in the Josephson junction region and hence there is no "inertia" connected with its variation (especially in a tunnel Josephson junction). The role of inertia in the case of the Josephson junction is played by the capacitance. Indeed, when the capacitance is zero (overdamped Josephson junction) there is no hysteresis in the I-V characteristic. The same is true for the Ginzburg-Landau model [Eqs. (2.1)] in the limit $\tau_{|\psi|} \to 0$ (when, for example, $u \to 0$).

The main properties we found for phase-slip centers may be obtained in the framework of the sample RCSJ (resistively and capacitevely shunted junction) model for the Josephson junction [18, 62] (see Fig. 2.3). We consider the overdamper limit (damping parameter β_c is small) because of its simplicity. For low frequencies we have a linear dependence of j_c on j_{ac} (at small amplitudes of the ac current) which changes to a nonlinear dependence at high frequencies. We also have oscillations in $j_c(j_{ac})$ with the same qualitative behavior (see discussion two parameters above) when one changes the period or amplitude of the e.m. radiation. The main differences are (i) the absence of discontinuous jumps in j_{c1} which we found for some frequencies and (ii) there is almost no decay in the amplitude of the oscillations of j_{c1} with j^{ac} (compare Figs. 2.2 and 2.3) [69] [Ref. 16]. The latter feature is connected with the existence of the third critical current at which the phase-slip process decays in the superconductor. Actually it is related to the problem of the stability of the boundary between the superconductor (S) and the normal (N). It has been known for a long time (see the review in Ref. [65], for example) that in the presence of transport current the S-N boundary is unstable an it should move in the direction of the

normal metal (and recover superconductivity in the sample) at $j < j_{c1}$ and it moves in the direction of the superconductor (and destroy superconductivity) at $j > j_{c3}$. In the range $j_{c1} < j < j_{c3}$ the phase-slip process exists.

In Ref. [32] the physical meaning of the current j_{c1} was studied. Here we try to clarify the meaning of the current j_{c3}. Using Eq. (2.1) we may write the equation for the dynamics of the magnitude of the order parameter:

$$u\sqrt{1+\gamma^2|\psi|^2}\frac{\partial|\psi|}{\partial t} = \frac{\partial^2|\psi|}{\partial s^2} + |\psi|(1-T-|\psi|^2-p^2). \tag{2.4}$$

From this equation it follows that the order parameter decreases in time (and hence the normal phase grows) if the right-hand side of Eq. (2.4) is negative. We may estimate the term -$p^2|\psi|$ (the other terms lead to a positive contribution) via the equation for the electrostatic potential, Eq. (2.2), $j = j_n + |\psi|^2]p$, and from the knowledge that the normal current density decays in the superconductor as $j_n = je^{-x/\Lambda_Q}$ in the absence of the Andreev reflection process (see ref. [70], for example). Λ_Q is the decay of the charge imbalance in the superconductor and within the framework of Eq. (2.1), $\Lambda_Q \sim \sqrt{\gamma/u}(1-T)^{1/4}$ [in the limit $\gamma(1-T)^{1/2}$]. Because the variation of the order parameter occurs on a distance of about ξ (it is the size of the S-N boundary) and in the above limit $\Lambda_Q \gg \xi$, we have $|\psi|^2 p \simeq j/\Lambda_Q (j_n \sim j - j/\Lambda_Q)$

$$u\gamma|\psi|\frac{\partial|\psi|}{\partial t} = \frac{\partial^2|\psi|}{\partial s^2} + |\psi|(1-T-|\psi|^2) - \frac{j^2}{\Lambda_Q^2|\psi|^3}. \tag{2.5}$$

Supposing that the distribution of the order parameter slightly depends on the actual distribution of the normal currents density near the S-N boundary, we find [assuming that $\psi \sim (1-T)^{1/2}$]

$$j_{c3} \simeq \Lambda_Q(1-T)^{3/2} \sim \sqrt{\gamma/u}(1-T)^{5/4} j_0(T=0). \tag{2.6}$$

This expression should be considered only as a rough estimate to clarify the dependence of j_{c3} on the parameters γ and u. It explains why with increasing γ oscillations decay slower (see Fig. 2.2) and the partially superconducting (resistive) state could exist at higher currents with decreasing u as recently found numerically in Ref. [71].

Because of the existence of a finite j_{c3} (which is absent in the sample RCSJ model of the Josephson junction), oscillations in j_{c1} decay for large enough amplitudes of the ac current. Another reason for the fast (in comparison to the Josephson junction case) decay may be related to heating effects. Due to heat dissipation, the local temperature of the superconductor may strongly deviate from the bath temperature. In Fig. 2.4 we present the dependences of j_{c1} and j_{c2} for different regimes of heat removal from the sample. It is clear that for the case of weak heat removal oscillations decay much faster. This is due to local increase of temperature (which is not necessary above T_c) and hence to a decrease of j_{c3} according to Eq. (2.6).

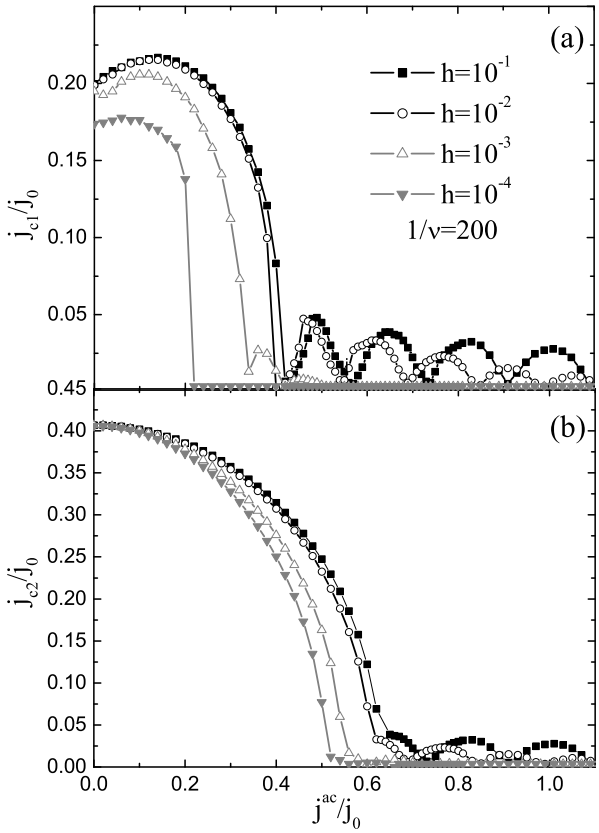

Fig. 2.4: Dependences of j_{c1} (a) and j_{c2} (b) on the amplitude of the ac current at different values of the heat removal coefficient. Current j_{c2} dependence on the heat dissipation (for $j^{ac} < 0.5$) due to the presence of the ac electric field in the superconducting state (even in the absence of the phase slips) and hence normal component of the current.

2.3.2 B. asymmetric ac signal

Interesting effects occur when we apply e.m. radiation which is asymmetric in time. Namely, we considered the case in which the ac current contains a second harmonic which is phase shifted with respect of the first harmonic:

$$j(t) = j^{dc} + j_1 \sin(2\pi\upsilon t) + j_2 \sin(4\pi\upsilon t + \theta_0). \tag{2.7}$$

We found that such a current may lead to a nonzero-voltage response even if the dc current is equal to zero. This effect is similar to the one which was theoretically predicted in Refs. [72] and [73] and experimentally found in Ref. [15] for the ratchetlike behavior of a single Josephson vortex in an annular Josephson junction. In Fig. 2.5 we present the dependence of the voltage induced in the superconductor by the current [18] as a function of the dc current j^{dc} for $j_1 = 0.5$, $j_2 = 0.3$, and $1/\upsilon = 4000$ [Fig. 2.5(a)] and $1/\upsilon = 200$ [Fig.2.5(b)].

If we apply a current [18] with no dc component and with a high enough frequency, then for relatively small amplitudes j_1 and j_2 no phase slip are created in the sample (if we take the initial condition $|\psi| = 1$ or equivalently we start from a pure superconducting state in the experiment) and we have V=0. if now due to some external influence (e.g., a pulse of laser beam or in numerical calculations we put $\psi = 0$ in the center of the sample at t=0), superconductivity is locally weakened or destroyed, phase slip process in induced, and as a consequence we will observe a nonzero-voltage response. Alternatively, we can apply a high dc current (to nucleate phase slips) and decrease it to zero.

The value of the induced (or rectified) voltage at $j^{dc} = 0$ strongly depends on the phase θ_0 (see Fig. 2.6). In comparison to the work of Ref. [15] the rectified voltage is nonzero even for $\theta_0 = 0$ (for $1/\upsilon < 10^4$). The reason is that for phase-slip processes the "damping" parameter (using the terminology for Josephson junctions) and the characteristic times are large and the system behaves in an adiabatic was only for relatively low frequencies (for the parameters of Fig. 2.6 at $1/\upsilon > 10^4$).

2.4 DISCUSSION

Let us estimate the experimental conditions under which the predicted effects can be observed. In the case for low temperature superconductors the critical temperature is about several kelvins and $\tau_{GL}(0) \sim 5.2 \times 10^{13} s/T_c$. The predicted effects therefore should be observable in the GHz range of e.m. radiation at temperatures not too so close to T_c (to exclude heating of the sample by large currents). Actually part of our theoretical results was recently observed in an experiment [60] on tin bridges (with length $5\mu m$) and width $2\mu m$) at a temperature close to $T_c \sim 3.8K$ and for not very large incident power of radiation (in our units for $j^{ac} < 0.5 j_0$). The nonmonotonous dependence of the $j_{c1}(j^{ac})$ [similar to that shown in Fig. 2.1(a)] was found at $\upsilon = 200MHz$ and T=3.67 K, and the critical current j_{c2} decayed always with increasing j^{ac} unless simulation of superconductivity occurred at $\upsilon > 3GHz$. besides, discontinuous jumps in the dependence $j_{c1}(j^{ac})$ (see Fig. 2.2) were observed at high frequencies $v_c \simeq 1/\triangle V$ (in experiment $v_c \sim 9.3GHz$) when transition to

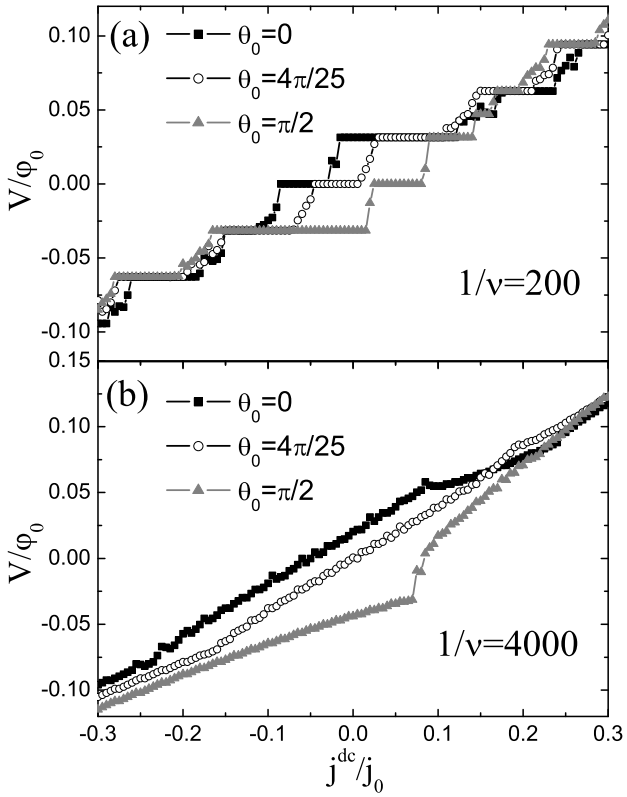

Fig. 2.5: Current-voltage characteristics of the superconducting sample in the presence of a time asymmetric ac signal. Eq. (2.7) ($j_1 = 0.5$, $j_2 = 0.3$, $\gamma = 40$), with the period $1/\nu = 4000$ (a) and $1/\nu = 200$ (b). At chosen values for j_1, j_2 and period $1/\nu = 200$ phase slips do not nucleate at zero dc current if we start from the superconducting state. Therefore, at some moment in time we locally suppress superconductivity which leads to the nucleation of phase slips.

the zero-resistance state occurs in the Shapiro step. the rest of our theoretical results (for $j^{ac} \gtrsim 0.5 j_0$) still need experimental verification.

We showed that applying a time asymmetric ac signal to the superconducting film may induce a finite voltage even in an unbiased system $j_{dc} = 0$ (Fig. 2.6). As a consequence one may use it a as a rectifier or voltage source of high precision at high frequency $\upsilon_c > 2e\triangle V/\hbar$ of radiation. The actual value of the

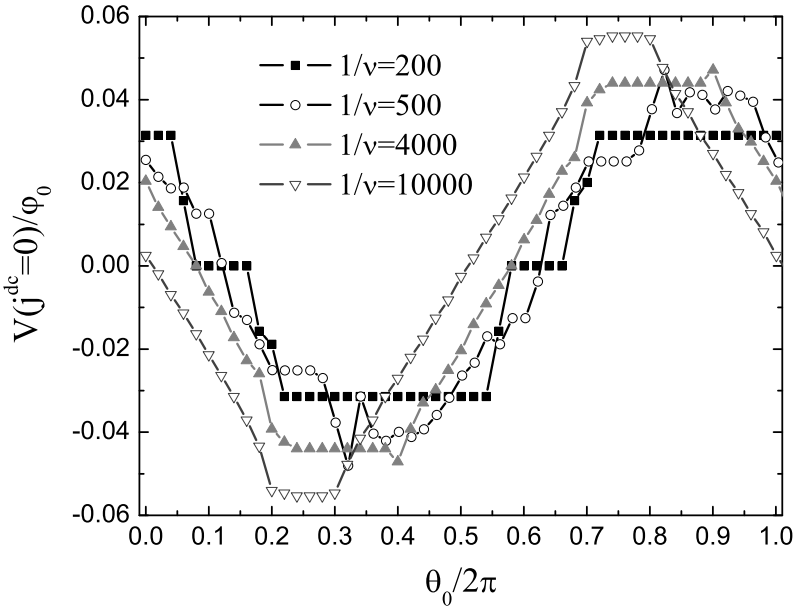

Fig. 2.6: Dependence of the induced voltage for $j^{dc} = 0$ on the phase shift between the two ac signals θ_0 for different frequencies ν of the ac signal (parameter as in Fig. 2.5). In comparison with Ref. a nonzero voltage appears already for θ_0 in the case of high frequencies. This is connected with the strong nonlineariity of the studied system and the dependence of the different relaxation times on the applied current. It is interesting to note that for frequencies close to, or larger than, $\nu_c = 2e\Delta V/\hbar$ the induced voltage is proportional to the frequency of the applied signal.

induced voltage is in the range of several μV per phase slip center (for low-temperature superconductors at T close to T_c). In our calculations we restricted ourselves to the case when only one phase-slip centers arises in the system. If several phase-slip centers coexist, they will start to interact with each other and such a system may be synchronized [61]. Consequently the rectified quantized voltage may increase several times in magnitude. Such a quantized voltage was already observed experimentally in unbiased tunnel Josephson junctions [74, 75]. and used for measuring the ratio $\hbar/e$ and as a standard for the voltage [62].

As we already pointed out above, the behavior of the phase-slip center under the influence of the e.m. radiation is very similar to the behavior of a

Josephson junction. The critical currents decay and oscillate with increasing the amplitude of the ac current and have a similar dependence on the frequency of the applied radiation (compare Fig.s 2.2 and 2.3). the main differences are the faster decay and jumps in the dependence $j_{c1}(j^{ac})$ (Fig. 2.2) in comparison to the case of a Josephson junction. We may understand this by the influence of the transport current on the value of the order parameter (instability of the S-N boundary at finite current j_{c3}) and the existence of the finite-voltage jump $\triangle V$ in the current-voltage characteristics and hence the low threshold for the intrinsic frequency of the phase-slip process. Both these effects are absent in the RSJ model with fixed Josephson critical current I_{c0} and zero capacitance.

Publications. The results presented in this chapter were published as:

- D. Y. Vodolazov, A. K. Elmurodov, and F. M. Peeters, *Critical currents of the phase slip process in the presence of electromagnetic radiation: Rectification for time assymetric ac signal*, Phys. Rev. B **72**, 134509 (2005)

3

Phase slip phenomena in NbN superconducting wires with leads

3.1 INTRODUCTION

It is known that phase-slip centers (PSC) occur in the resistive state of long quasi-one-dimensional channels [76] states have been investigated on "one-dimensional" samples, *e.g.* whiskers [13] and microbridges [12] exhibiting phase-slip centers [26]. A dissipative state has a resistance significantly below the normal state value. In one or more areas along the wire a phase-slip is created which is a region (with size about coherence length ξ) of dynamically suppressed order parameter ξ and surrounded by diffusive tails where the quasiparticles and Cooper pairs have different electrochemical potentials (providing a local charge imbalance). The diffusion length associated with the relaxation time for this specific nonequilibrium effect determines the effective resistance of the phase-slip center.

Recently experiments on superconducting nanowires [77] have attracted renewed attention on the elecrical and magnetic manifestations of thermal and quantum fluctuations. The successive nucleation of PSC leads to the appearance of a stairlike structure in the I-V characteristics [32]. The existence of phase-slip centers was confirmed in low temperature superconductors [78]. Recently phase-slip centers were observed [79] in the presence of an external applied magnetic field. It was shown in Ref. [80] that with attaching many low-resistance Ohmic contacts along the electrodeposited Sn nanowires one can

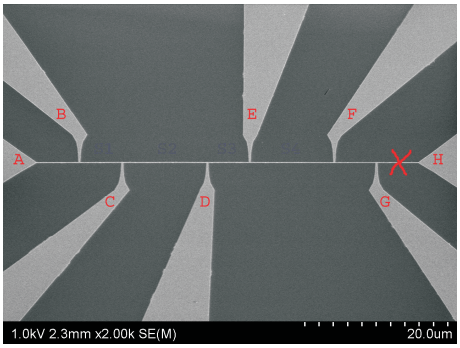

Fig. 3.1: A scanning electron microscopy image of a NbN nanowire with attached current and voltage electrodes. Segment GH is broken.

perform electrical measurements on different segments of the superconducting wire. It is also often pointed out that phase-slip lines in wide films are similar to phase-slip center in narrow films [81, 82].

In this section we present experimental results on current-voltage characteristics of a mesoscopic superconducting NbN wire with many superconducting contacts (see Fig. 3.1). In this geometry, the contacts play a very important role because they make it possible to study experimentally the size effect on the phase-slip phenomena. The effect of the sample length on the formation of the phase-slip centers is studied within the time-dependent Ginzburg-Landau (GL) theory. The GL equation when it coupled to the heat diffusion equation because of inevitable heat dissipation, which can lead to a local transition to the normal state.

3.2 EXPERIMENTAL RESULTS

The sample was fabricated as follows: thin NbN films were deposited from a Nb target by DC magnetron sputtering on a Si/SiO_2 substrate at room temperature in a 8.55 mTorr Ar/N_2 atmosphere (gas flow: 38.2 and 2.43 sc cm, respectively). This process yields typically $T_c = 10K$ and $\xi \sim 5$ nm for film thickness of a few tens of nm. The NbN films were patterned to form the structure shown in Fig. 3.1 by $SF6$ reactive ion etching using a 10-20 nm thick Al_2O_3 mask. The pressure and the bias for the $SF6$ etch are chosen such that the Al_2O_3 is not damaged. This Al_2O_3 mask is subsequently removed with NaOH. The multi-contacts are thus of the same nature than the strip under study and are labeled A,B,C,... as shown in Fig. 3.1 from left to right. Samples were cooled to helium boiling temperature in a cryostat and each measurement

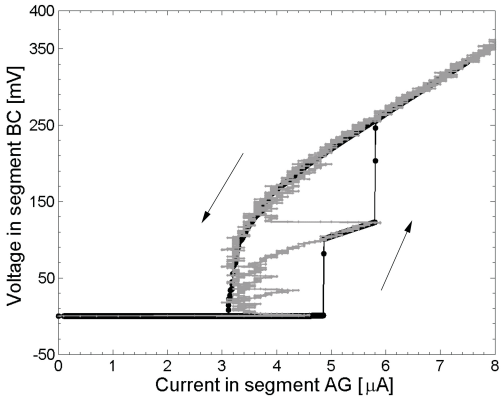

Fig. 3.2: Voltage-current characteristic of BC segment ($6\mu m$ long, 70 nm wide and 75 nm thick; four contacts) of the sample (see Fig. 3.1) under current drive (black curve) or voltage drive (gray curve) condition. Base temperature is 4.2K and no external magnetic field is applied.

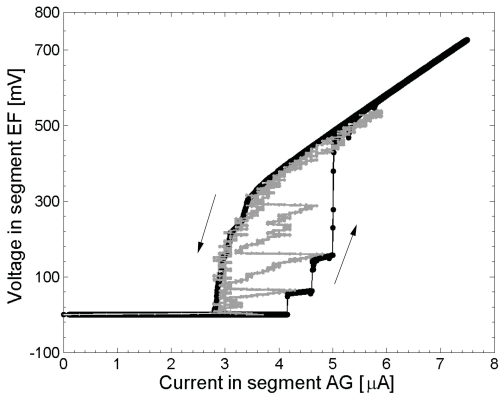

Fig. 3.3: The same as Fig. 3.2 but for the segment EF ($12\mu m$ long 70 nm wide and 75 nm thick) in Fig. 3.1

line was filtered using pi filters. Current or voltage bias was applied to each segment using a 4 contact configuration.

Figs. 3.2 and 3.3 present the current-voltage properties of two segments (respectively, 6 and 12 μm long) of the wire. Their normal state resistance just above T_c is quite high ($8.5k\Omega/\mu$m), which is characteristic for such a hard superconductor. As a consequence there is Joule heating but the relatively good cooling from the leads and the substrate allows avoiding the formation of a self-spreading hotspot [12] in current bias when the critical current is reached. Rather with current sweep up, resistive domains appear successively and they

can be stabilized in a wide current range. Comparing Figs. 3.2 and 3.3, we also notice that the total number of these resistive domains scales with the length of the segment. Applying the voltage (gray curves in Figs. 3.2 and 3.3), we see that even more of such nonequilibrium regions can be formed in the segment than the current drive suggest. This indicates the possibility of obtaining different number of such normal regions simultaneously. In a current sweep down a continuous behavior is found without any jump between different resistive states.

Fig. 3.4 shows the I-V curve of another, shorter, segment, measured with only 2 contacts. It has a smaller normal state resistance (5.3 kOhm/μm). The resistance of the contact being small, the initial part of the curve before the first critical current consists mainly of a typical vortex region. Due to the Lorentz force that acts on the trapped or self-induced vortex as the current is increased, a flow of Abrikosov vortices is preceding the formation of the resistive domain [83]. The high number of successive resistive domains in this smaller and shorter segment is probably linked to a better cooling combined with a smaller Joule effect.

Due to the regularity of our samples, as illustrate in Fig. 3.1, we feel that heating cannot be responsible for the formation of these various domains (although it probably affects them). Indeed, pure hotspots would tend to coalesce as the current is raised. Therefore, the formation of phase-slip lines is a natural mechanism to think of in view of our results, even if they are observed here far from the critical temperature. Given the similarities between phase-slip line and phase-slip center, this is not surprising since phase-slip centers have also been observed far from T_c. Therefore, it makes sense to compare these results to the theoretical model of phase-slip center in which the heating effect is included.

3.3 THEORETICAL MODEL

For our theoretical study we use the generalized time-dependent Ginzburg-Landau (TDGL) [14, 15] equation to describe the order parameter in the wire:

$$\begin{aligned}\frac{u}{\sqrt{1+\gamma^2|\psi|^2}}(\frac{\partial}{\partial t}+i\varphi+\frac{\gamma^2}{2}\frac{\partial|\psi|^2}{\partial t})\psi \\ =(\bigtriangledown-i\mathbf{A})^2\psi+(1-T-|\psi|^2)\psi,\end{aligned} \tag{3.1}$$

which is supplemented with the equation for the electrostatic potential

$$\Delta\varphi = div\{Im[\psi^*(\nabla-i\mathbf{A})\psi]\}. \tag{3.2}$$

Here there is an explicit inclusion of the time relaxation τ_ϵ (through the coefficient $\gamma = 2\tau_\epsilon\triangle_0/\hbar$) for the nonequilibrium quasiparticle distribution due

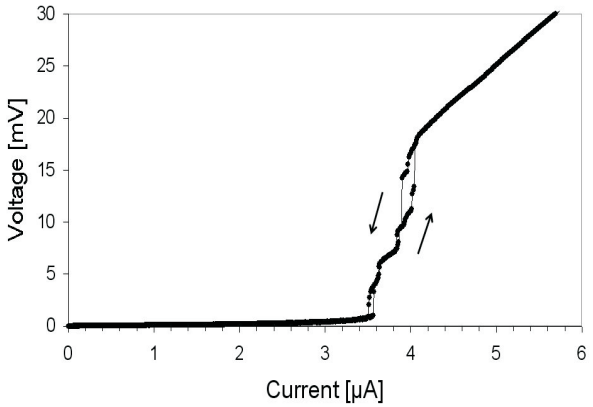

Fig. 3.4: Voltage-current characteristic of the NbN segment ($1\mu m$ long, 60 nm wide and 50 nm thick) under current bias condition with two contacts. Base temperature is 4.2K and there is no external magnetic field.

to interaction and $\triangle_0 = 4k_BT_c/u^{1/2}\pi$ is the "effective" value of the order parameter at $T = 0$. In Eq. (3.1) all the physical quantities (order parameter $\psi = |\psi|e^{i\phi}$, electrostatic potential φ) are measured in dimensionless units: the momentum of superconducting condensate $p = \nabla\phi$ is scaled by the unit $\Phi_0/[2\pi\xi(0)]$ (where Φ_0 is the quantum of magnetic flux), the order parameter is in units of $\triangle_0$, and the coordinates are in units of the coherence length $\xi(0) = (8k_BT_c/\pi\hbar D)^{-1/2}$ (D is the diffusion constant). In these units the current density is scaled with $j_0 = \sigma_n\hbar/2e\tau_{GL}(0)\xi(0)$, the time is in units of the Ginzburg-Landau relaxation time $\tau_{GL}(0) = \pi\hbar/8k_BT_cu$, and the electrostatic potential φ is in units of $\varphi_0 = \hbar/2e\tau_{GL}(0)$ (σ_n is the normal-state conductivity). The vector potential is equal to zero because there is no applied magnetic field and self-induced effects are small for our system.

To simulate the real experimental situation we considered a superconducting wire with two attached leads, as illustrated in the inset of Fig. 3.5. Here we present our results obtained for the temperature $T = 0.9T_c$ and for the parameters $u = 5.79$ and $\gamma = 40$ [15]. To simulate a real experimental situation we use "bridge" boundary conditions $|\psi(-L/2)| = |\psi(L/2)| = 1$, $\psi(\pm L/2, t + dt) = \psi(\pm L/2, t)\exp^{-i\varphi(\psi(\pm L/2)dt)}$, and implemented the boundary condition $\partial\psi/\partial x = 0$ at the contacts and $\varphi(-L/2, t) = 0$. Initial conditions were $|\psi| = 1$ and $\varphi = 0$. The behavior of the system is studied on a large time scale when time-averaged values no longer depend on time.

The superconducting wire is thermally conducting: since the electronic contribution to this thermal conductivity is very small for NbN at low T, the thermal conductivity is close to its value in the normal state. Thus the wire will carry away the generated heat as well as the substrate. Therefore, we have

to couple the TDGL equation to the temperature diffusion equation. We solved the equation for the temperature distribution in the sample:

$$C_{eff}\frac{\partial T}{\partial t} = k_{eff}\triangle T + j_n^2 - h_c(T - T_0), \tag{3.3}$$

where $C_{eff} = (D_sC_s/d_f + C_f)T_c\sigma_n/\tau_{GL}(0)j_0^2$, $k_{eff} = (D_sk_s/d_f + k_f)T_c\sigma_n/\xi^2 j_0^2$, $h_c = k_sT_c\sigma_n/D_cd_fj_0^2$, the heat transfer coefficient h_c governs the heat removal from the sample, and C_s, C_f, k_s, and k_f are heat capacity and heat conductivity of the substrate (subscript s) and film and sample (subscript f), respectively. Here we used a model for the temperature distribution in thin superconducting films as was previously discussed in details in Ref. [64] and we assumed that the thickness of the substrate and film, $D_c + d_f$, is much smaller than the healing length $\Lambda_h = \sqrt{k_{eff}/h} \gg D_s + d_f$. If $D_sC_s/d_f \ll C_f$ and $D_sk_s/d_f \ll k_f$, we can use the Wiedermann-Franz law as an estimate for C_f and k_f and we obtain for $C_{eff} = \pi^3/48 \simeq 0.65$ and $k_{eff} = \pi^4/48u^2 \simeq 0.06$ at temperature close to T_c. Because of the uncertainty in the actual values of C_s and k_s we used following values: $C_{eff} = 2.0$ and $k_{eff} = 0.0003$. We checked that our results only weakly depend on our choice of C_{eff} and k_{eff}. We also put $A = 0$ in Eqs. (3.1) and (3.2) because we considered the one-dimensional model, in which the effect of the self-induced magnetic field is negligible and we assume that no external magnetic field is applied.

3.4 NUMERICAL RESULTS

In this section we present our theoretical results about transport properties of the system in the current driven regime. Let us first consider the effect of the wire length on the I-V characteristics of the system. Fig. 3.5 shows the I-V curve of the sample with length $L = 70\xi$ for both increasing (open symbols) and decreasing (filled symbols) currents. With increasing the applied current the system switches to the first resistive state with a jump in the voltage at the upper critical current $j_{c2} = 0.3j_0$. At this value of the current one phase-slip enters the sample leading to finite resistance of the sample. Because of the chosen geometry the phase-slip center appears always in the center of the sample where the order parameter is minimal (see Fig. 3.6(a)). Because of the heat transfer the local temperature increases in the phase-slip centers (see Fig. 3.6(c)). With further increasing the current the frequency of the order parameter oscillations increases leading to a larger time average voltage over the wire. Finally our observe the jump to the normal state and destruction of superconductivity over the whole sample.

If we start from the normal state and decrease the current the superconducting state is nucleated at the current $j_{c1} = 0.11j_0$, which is much smaller than j_{c2}, i.e. the system exhibits a clear hysteresis similar to what we obtained experimentally (see Fig. 3.2). For decreasing current the superconducting state

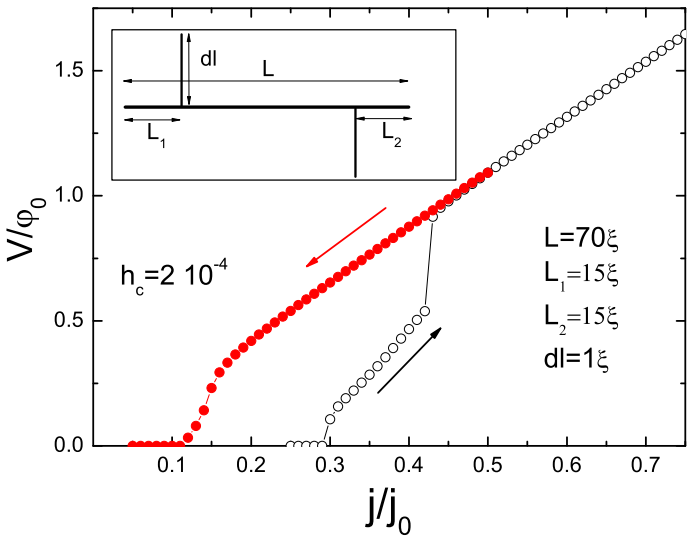

Fig. 3.5: Current-voltage characteristic of a superconducting wire of length $L = 70\xi$ with two attached leads of size $dl = 1\xi$ for increased (open circles) and decreased (filled circles) applied currents. The distances from the two edges of the wire to the leads are $L_1 = L_2 = 15\xi$. The inset shows a schematic view of our model system.

is not recovered at a current $j_{c1} < j < j_{c2}$ because of the high resistance which leads to larger heating of the sample. Note that no jumps in the $I - V$ curve is found in the current sweep down regime, which agrees with the experimental results.

Fig. 3.7 shows the $I - V$ curve of a much longer with size $L = 150\xi$ in the two current sweep regimes. The other parameters of the sample are the same as for the one in Fig. 3.5. It is seen from this figure that the number of voltage jumps in the I-V curve increases with increasing the length of the wire, which is in good agreement with our experiment (see Figs. 3.2 and 3.3). The latter is due to the fact that a longer wire can accommodate a larger number of phase-slip centers while remaining in the superconducting state. As shown in Figs. 3.6(b,d), phase-slip centers appear in two places in the sample. Although the number of phase-slip centers increased with increasing the length of the wire, the second critical current j_{c2} and the current corresponding to the superconducting-normal state transition remains the same. However, the first critical current j_{c1} slightly decreases with increasing the size of the wire

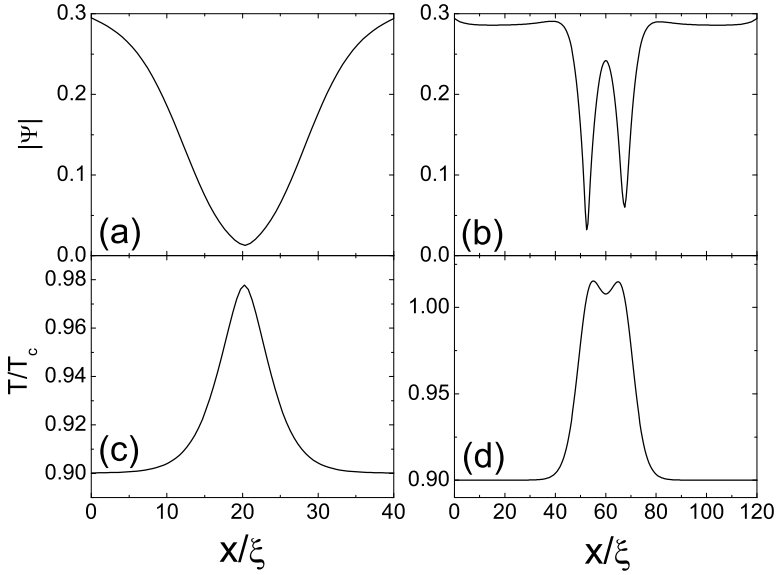

FIG. 3.6: The time average modulus of the order parameter $|\psi|$ (a,b) and temperature (c,d) between the two contacts $L_1 = L_2 = 15\xi$. The length of the wire is $L = 70\xi$ (a,c) and $L = 150\xi$ (b,d); the applied current density is $j = 0.3j_0$ (a,c) and $j = 0.4j_0$ (b,d).

(compare with experimental results in Fig. 3.2 and 3.3). With current sweep down there are again no voltage jumps in the I-V curve (compare with Fig. 3.2 and 3.3). As was shown in Ref. [33] the voltage jump at $j = j_{c1}$ depends on temperature roughly as $\Delta V \sim \hbar/(e\tau_{epsilon})(1 - T/T_c)^{1/2}$ near the critical temperature and hence local heating strongly decreases this voltage jump.

Next we study the influence of the heat transfer coefficient h_c to the obtained results. As an example, we plotted in Fig. 3.8 the I-V curve of the sample considered in Fig. 3.7 but for two different heat transfer coefficients that amount to $h_c = 2 \times 10^{-3}$, ($h_c = 2 \times 10^{-2}$) which is 10 (100) times larger than the one in Fig. 3.7. It is seen that the behavior of the curve for increasing current is the same as in Fig. 3.7. However, in this case the curve for decreasing current changes drastically: jumps appear indicating the presence of phase-slip centers in the sample. If the heat transfer coefficient increases by 100 times the one in Fig. 3.7, first, the number of voltage jumps in the current sweep up regime increases considerably. Second, the finite size steps in the I-V characteristics are found even for decreasing currents. Finally, the first critical current j_{c1}

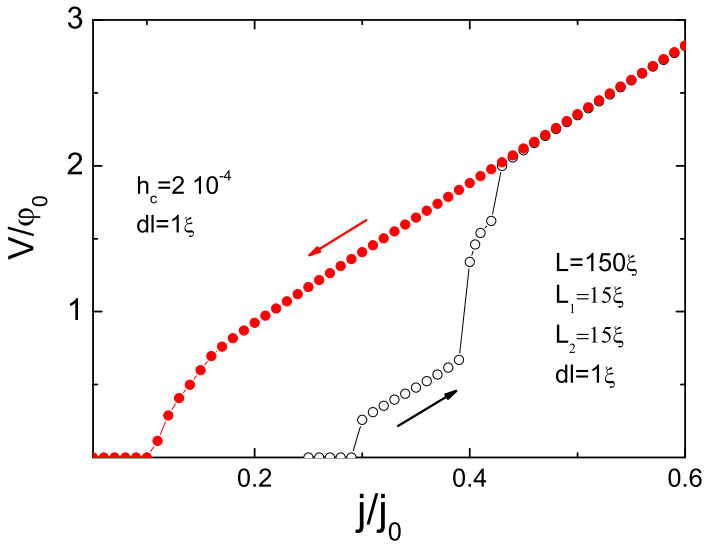

Fig. 3.7: The same as Fig. 3.5 but now for a longer wire with length $L = 150\xi$.

considerable increases with increasing h_c. The reason for such changes is that when we increase h_c, the heat removal from the system increases and there is practically no local temperature increase due to the formation of phase-slip centers. As a result the decay length of the electric field is small and there is place in the wire for many phase-slip centers.

3.5 CONCLUSION

We have studied transport properties of a superconducting NbN wire with many contacts attached allowing us to perform transport measurements in different segments of the wire. The system exhibits clear hysteresis with finite jumps in the I-V curve. Each jump corresponds to phase-slip lines entering the sample, which was confirmed by numerical simulations using the time-dependent GL theory. The number and size of these jumps strongly depends both on the dimensions (*i.e.* length of the wire) and the heat transfer properties of the system. The value of the superconducting-normal transition current increases with increasing both the sample size and the heat transfer coefficient, whereas the critical current for the entrance of the first phase-slip remains the same.

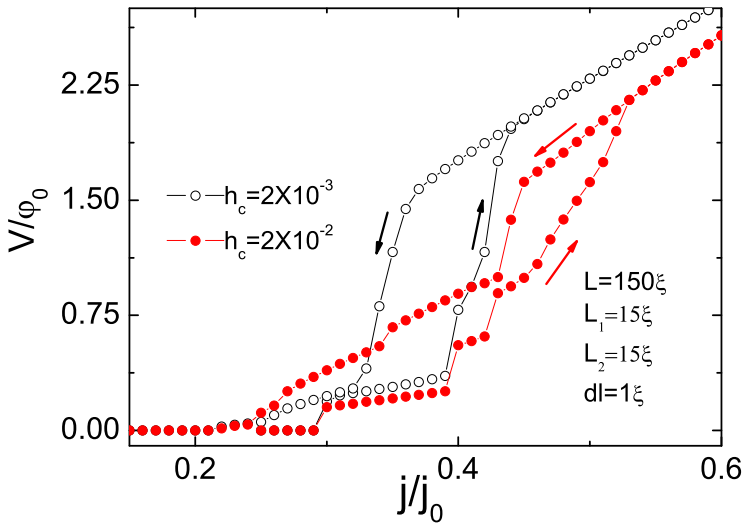

FIG. 3.8: The same as Fig. 3.7 but now for heating transfer coefficients $h_c = 2{\cdot}10^{-3}$ (open circles) and $h_c = 2 \cdot 10^{-2}$ (filled circles).

Our numerical calculations show that the heating is not obligatory leads to complete destruction of superconductivity (as for example was supposed in Ref. [6]), but instead may provide changes in superconducting propreties due to local increase of temperature. For example the size of the phase slip center increases with temperature and it can qualitatively explain the presented experimental results.

- A. K. Elmurodov, D. Y. Vodolazov, F. M. Peeters, S. Michotte, S. Adam, F. de Menten de Horne, L. Piraux, D. Lucot, D. Mailly, *Phase-slip phenomena in NbN superconducting nanowires with leads* (submitted to Phys. Rev. B.).

4

Finite size effect on the resistive state in a mesoscopic type-II superconducting stripe

4.1 INTRODUCTION

When a thin superconducting film is placed in a perpendicular magnetic field that is larger than some critical value, Abrikosov vortices penetrate the sample and form a triangular vortex lattice in the absence of pinning. If now a transport current is applied to the sample vortices start moving under the action of the Lorentz force of the current. The vortex motion leads to energy dissipation in the system and to a finite voltage and electrical field in the superconductor. At large vortex line velocities, the vortex motion becomes unstable and a nonequilibrium distribution of the quasiparticles appear, due to the slow energy relaxation, which leads to an electronic instability and an abrupt switching into a state with higher electrical resistivity, i.e., the voltage-current characteristic exhibits a hysteretic jump, as predicted by Larkin and Ovchinnikov (LO) [38]. The electric field due to vortex motion results in a decreasing size of the vortex cores because quasiparticles accelerated by the electrical field can reach energies above the superconducting energy gap and diffuse away from the vortex core.

Electric-field induced flux flow instabilities intensively studied in the past both in low [39–42] and high [43–47] temperature superconductors, in general agree reasonably well with the LO theory. However, in some cases, the LO theory turns out to be insufficient to describe the experimental results. For

example, at low temperatures the LO description breaks down, suggesting a different origin for the flux flow instabilities [41]. Explanation for the flux flow instabilities beyond the original or modified LO picture were sought in dynamic vortex lattice crystallization [48], depinning phenomena [49], apperance of hot spots [50], and recently in vortex core expansion due to electron heating at low temperatures [51].

However, in the original LO theory the question about vortex structure before and after the transition was not considered. At the end of the 70s it was speculated that lines with fast vortex motion (so called phase slip lines) should appear in the superconductor at the transition point. Because analytical calculations are strongly restricted due to the mathematical complexity of the problem, only a semi-quantitative analysis was made using the assumption that phase slip lines already exist in the sample [52].

A number of works have been published were vortex motion was studied theoretically using a numerical simulation of the extended time-dependent Ginzburg-Landau (GL) equations [53–56] where the time τ_{in} of the nonequilibrium quasiparticle distribution function was explicitly included. In Refs. [53, 54] two types of vortex motion were found: slow and fast vortex motion (the latter was named the kinematic vortex [54]). However, neither the influence of the magnetic field nor the transition between these types of motion nor the transformation of the vortex lattice were addressed. In Ref. [55] the deformation of the vortex core due to the finite relaxation time of the order parameter was found and a short range attraction between vortices was predicted. In a recent paper [56] the rearrangement of the vortex lattice due to the above effect and the transition from the slow to the fast vortex motion (phase slip line) were studied for an infinitely long superconducting slab placed in a parallel magnetic field.

In this chapter of the thesis we investigate nonequilibrium processes in a mesoscopic superconducting stripe in the presence of a perpendicular magnetic field and a transport current. The effect of the finite size of the sample, as well as the effect of the normal contacts on the current-voltage characteristics of the sample are considered. Due to the finite length of the strip and the intrinsically nonuniform current distribution along the sample (because of normal current contacts - see Fig. 4.1) we do not have any degeneracy in our model with the system of periodical boundary conditions as reported in Ref. [56].

4.2 THEORETICAL MODEL

We consider a very thin (thickness $d \ll \xi,\ \lambda$) superconducting strip (length L, width W) in the presence of a perpendicular magnetic field with a transport electric current applied through the normal contacts (size a) (see Fig. 4.1). In the case of thin films the self induced magnetic field can be neglected (no

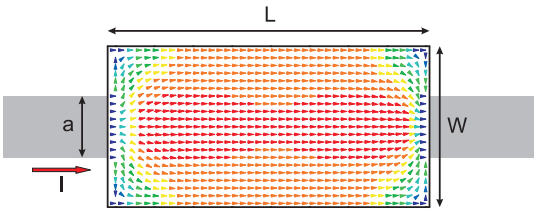

Fig. 4.1: A schematic view of the studied superconducting strip with attached normal leads. Vector plot shows the distribution of the superconducting current in the sample in case of $H = 0$ and nonzero applied transport current. Red/blue regions correspond to high/low current.

demagnetization effect) and the generalized time-dependent Ginzburg-Landau (TDGL) equation can be written in the following form:

$$\frac{u}{\sqrt{1+\gamma^2|\psi|^2}}\left(\frac{\partial}{\partial t}+i\varphi+\frac{\gamma^2}{2}\frac{\partial|\psi|^2}{\partial t}\right)\psi = (\bigtriangledown - i\mathbf{A})^2\psi + (1-|\psi|^2)\psi. \tag{4.1}$$

This equation should be supplemented with the equation for the electrostatic potential

$$\Delta\varphi = \mathrm{div}\{\mathrm{Im}[\psi^*(\nabla - i\mathbf{A})\psi]\}, \tag{4.2}$$

which is nothing else than the condition for the conservation of the total current in the wire, i.e., div$\mathbf{j} = \mathbf{0}$. Here the parameter $\gamma = 2\tau_{in}\Delta(T)/\hbar$ is the product of the inelastic collision time τ_{in} for electron-phonon scattering where $\Delta(T) = 4k_BT_cu^{1/2}/\pi\sqrt{1-T/T_c}$ is the value of the order parameter at temperature T which follows from Gor'kov's derivation [84] of the Ginzburg-Landau equations. In Eqs. (1) and (2) all the physical quantities (order parameter $\psi = |\psi|\exp(i\phi)$, vector potential $\mathbf{A}$ and electrostatical potential φ) are measured in dimensionless units: the vector potential $\mathbf{A}$ and the momentum of the superconducting condensate $\mathbf{p} = \nabla\phi - \mathbf{A}$ are scaled by the unit $\Phi_0/(2\pi\xi)$ (where Φ_0 is the quantum of magnetic flux), the order parameter is in units of $\triangle_0$ and the coordinates are in units of the coherence length $\xi(T)$. In these units the magnetic field is scaled by $H_{c2} = \Phi_0/2\pi\xi^2$ and the current density by $j_0 = c\Phi_0/8\pi^2\Lambda^2\xi$. Time is scaled in units of the Ginzburg-Landau relaxation time $\tau_E = 4\pi\sigma_n\lambda^2/c^2 = 2T\hbar/\pi\triangle_0^2$, the electrostatic potential (φ) is in units of $\varphi_0 = c\Phi_0/8\pi^2\xi\lambda\sigma_n = \hbar/2e\tau_{GL}$ (σ_n is the normal-state conductivity). We also put $\mathbf{A} = (0, Hx, 0)$ in Eqs. (1) and (2) because we limit ourselves to the case where the effect of the current-induced magnetic field is negligible. The parameter u is equal to 5.79 in accordance with Ref. [**?**]. In our calculations we varied the other parameter γ from 0 to 20, which is proportional to the quasiparticle diffusion length λ_Q.

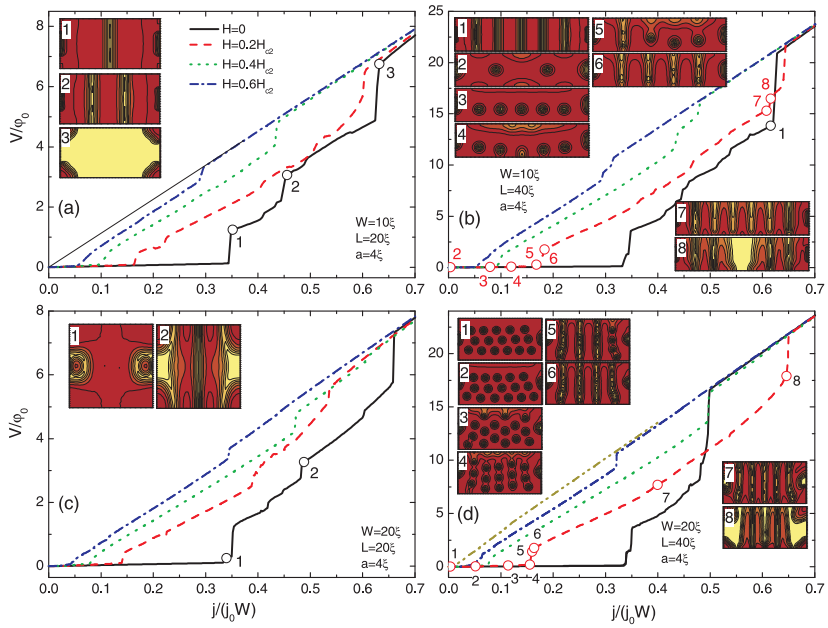

FIG. 4.2: Current-voltage (I-V) characteristics of a superconducting strip obtained in the current increasing regime at the magnetic fields: $H = 0$ (solid curve), $H = 0.2H_{c2}$ (dashed curve), $H = 0.4H_{c2}$ (dotted curve), and $H = 0.6H_{c2}$ (dash-dotted curve). The thin dotted line in (a) indicate the I-V curve of the sample in the normal state. The width of the sample is $W = 10\xi$ (a,b) and $W = 20\xi$ (c,d), the length is $L = 20\xi$(a,c) and $L = 40\xi$ (b,d), and the size of the normal contact is $a = 4\xi$. The insets show contour plots of the Cooper-pair density at a given time for the current values indicated in the main panel (red (dark gray)/light yellow (light gray) corresponds to high/zero Cooper-pair density).

Superconductor-vacuum boundary conditions $(\nabla - i\mathbf{A})\psi\,|_n = 0$, $\nabla\varphi\,|_n = 0$ at the boundaries of the sample and the normal metal-superconductor boundary conditions $\psi = 0$ and $\nabla\varphi\,|_n = -j$ at the contacts between the superconducting film with the normal leads are implemented in our simulations.

4.3 FINITE SIZE EFFECT ON THE RESISTIVE STATE

Let us first study the effect of sample dimensions on the formation of the resistive state. Fig. 4.2 shows the current-voltage I-V characteristics of a superconducting stripe for $\gamma = 20$ and for different values of the magnetic field. For zero magnetic field, first phase-slip line (PSL) enters the sample at some

critical current j_c in the middle of the sample, where the superconducting current reaches its maximum (inset 1 in Fig. 4.2(a)). This phase slip line leads to a finite jump in the I-V curve (point 1 in Fig. 4.2(a)). Contrary to phase-slip centers in 1D superconductors, the oscillations of the order parameter may not necessary be uniform along PSL: these oscillations may occur in the form of propagation of waves carrying the order parameter singularities across the film. Such waves (named kinematic vortices) have been discovered in numerical simulations using the 2D TDGL equations [54]. It was shown that [56] this phase-slip line, taken at an instantaneous time, consists of a line of counter propagating vortices and anti-vortices which are created on the opposite edge of the sample. These vortices and anti-vortices meet each other in the center of the sample where they annihilate. Averaged over time this line of vortices appear as a phase-slip line. The critical current j_c for the first phase slip line is independent on the dimensions of the sample for the given γ and equals to $j_c/(j_0 W) = 0.35$. After the appearance of the first phase slip line the superconducting current in its neighborhood is strongly suppressed on a distance of about the penetration depth λ_Q of the normal current (electric field) in the superconductor. As a result one needs a larger current to reach the condition for the nucleation of the next phase slip line in the strip. In general, the possible number of active PSLs is equal to the number of voltage steps in the corresponding I-V curve. Due to the symmetry of the sample more than one PSLs can penetrate the sample at the same time and tend to avoid those already in place (insets 2 in Fig. 4.2(c)). The number of those highly dissipative domains increases with increasing the sample dimensions (inset 1 in Fig. 4.2(b)). Because of the close proximity of the normal contacts superconductivity is locally suppressed (inset 1 in Fig. 4.2(c)) and phase slip lines can also be distorted (inset 1 in Fig. 4.2(c)). With further increasing the applied current the system transits to highly dissipative state with a normal path between the contacts (inset 3 in Fig. 4.2(a)). However, the resistance of this state can be different from the one of the normal state (thin dotted line in Fig. 4.2(a)), because superconductivity is preserved at the corners of the sample (see inset 3 of Fig. 4.2(a)).

When we apply a magnetic field vortices penetrate the sample and arrange themselves into a vortex chains in narrow samples (inset 2 in Fig. 4.2(b)) or into a triangular lattice for larger samples (inset 1 in Fig. 4.2(d)). As the applied current increases the surface barrier for vortices to enter the sample decreases and consequently, the number of vortices inside the sample can increase with increasing j (insets 3 in Fig. 4.2(b)). At the same time vortex lattice moves as a whole due to the Lorentz of the current (inset 2 in Fig. 4.2(d)). With further increasing current vortices are set into motion and they penetrate the sample from one side and exit from the other side of the sample (inset 3 in Fig. 4.2(d)). This motion of vortices lead to a small jump in the I-V curve at currents much smaller than the normal state transition current density j_{c2}. At the same time a rearrangement of the vortex lattice takes place and vortex rows are formed

(inset 4 in Fig. 4.2(d)). With further increasing current vortex channels, or phase slip lines, appear in the sample (inset 5 in Fig. 4.2(b)). The coexistence of fast and slow moving vortices is also possible (inset 5 in Fig. 4.2(d)). This PSL is a 2D analogue of the phase slip centers in superconducting wires [33], with the difference that here the order parameter may vary across the 2D wire. The physical reason for the appearance of these vortex lines is as follows: the moving vortices leave behind a wake of reduced $|\psi|$ because of non-equilibrium effects [55, 56], i.e. the condensate at a particular point needs a finite time to recover to its initial value after the passage of a vortex. This induces a short range vortex attraction along the wire on top of the normal isotropic vortex-vortex repulsion, resulting into an anisotropic effective vortex-vortex interaction. With further increasing the current more PSLs enter that sample (insets 7 in Figs. 4.2(b,d)), in some cases interpenetrating the previous ones . Therefore, the steps in the I-V curve become smaller compared to zero magnetic field regime. Before the systems transits to the normal state individual vortex channel start merging (inset 8 in Figs. 4.2(b,d)). Note also that the voltage jump corresponding to the appearance of a PSL (points 6 in Figs. 4.2(b,d)) is more pronounced than the jump due to vortex motion (points 3). Thus the PSL mechanism turns out to be more effective in producing resistance. At larger magnetic fields voltage jumps become smaller and eventually disappear in the I-V curve (see solid gray curve in Fig. 4.2(d)). Similar magnetic field dependence of the current-voltage characteristic was recently obtained experimentally in superconducting nanowires [42]. This behavior is explained by the fact that the magnetic field suppresses the order parameter everywhere in the sample, leading to an increase of quasiparticle diffusion length, and hence there is a lack of space for the coexistence of a larger number of PSLs in the sample [33].

For longer samples we found very interesting result that the superconducting (resistive) to normal state transition critical current density j_{c2} *increases* with applying weak magnetic field (compare solid black and dashed curves in Figs. 4.2(b,d)) − the system is in the phase-slip line state for larger values of the applied current. This effect disappears with further increasing the applied field. Shorter samples sustain larger applied currents at zero magnetic field (see Figs. 4.2(a,c)). To our understanding, this unusual magnetic field induced increase of the critical current effect is related to the nonuniform distribution of currents over the sample width [34, 35]. As we see from Fig. 4.2 the individual phase slip lines should merge together in order to form higher dissipative state, i.e normal state. When we apply a small magnetic field the screening currents induced by the magnetic field decreases the current density on one side of the sample and increases it on the other side of the sample. That decreased current will not be able to merge the phase slip lines and, therefore, the system stays in the phase-slip line state for larger applied current values. This effect disappears at larger magnetic field values because the magnetic field suppresses the superconducting order parameter.

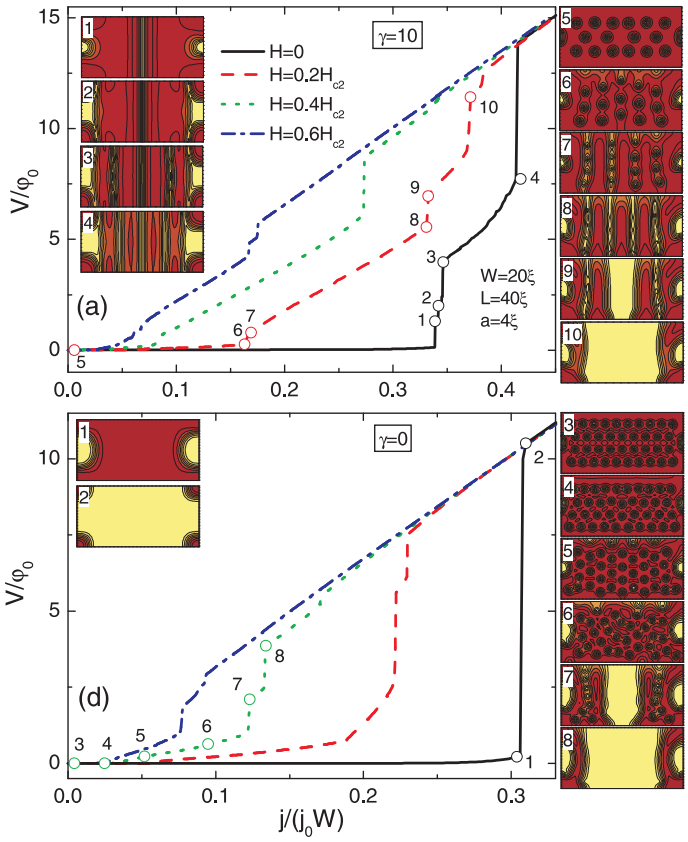

Fig. 4.3: The same as Fig. 4.2(d), but for $\gamma = 10$ (a) and $\gamma = 20$ (b).

4.4 EFFECT OF γ ON THE FORMATION OF PHASE SLIP LINES

In the GL framework, the effect of the parameter γ becomes very important in studying flux flow instabilities. When the PSL is present in the system, the electrical field decays over the quasiparticle diffusion length λ_Q, which is proportional to γ: $\lambda_Q \sim \sqrt{\gamma}$. Therefore, as γ increases the current range over which the PS solution is found actually increases to higher as well as to lower currents [15], i.e. the stability of the normal state becomes weaker. Moreover, the magnetic field range over which these states may exist also increases [56].

In what follows we study the effect of γ on the I-V characteristics of the sample. Fig. 4.3 shows the time-averaged voltage across the sample as a function of the applied current for $\gamma = 10$ (a) and $\gamma = 0$ (b) for different values of the applied field. The size of the sample is $L = 40\xi$ and $W = 20\xi$. Let us first discuss the case of $\gamma = 10$. At zero magnetic field phase slip lines

enter the sample and the number of these dissipative domains increases with increasing the applied current (insets 1-4 in Fig. 4.3(a)), as in the case of $\gamma = 20$ (see Fig. 4.2). If we apply a magnetic field, vortices penetrate the sample and arrange themselves into a deformed (due to the square symmetry of the sample) triangular lattice (inset 5 in Fig. 4.3(a)). The vortex lattice becomes distorted at small currents (inset 6 in Fig. 4.3(a)) and the vortices tend to align themselves more and more in line with increasing j (insets 6 and 7 in Fig. 4.3(a)). This rearrangement of the vortex lattice leads to an enhanced vortex density along the lines of vortices and lower density between those lines. In case when the number of vortices in the sample is fixed, by the given value of the field, the latter effect results in a decrease of the number of vortex lines (compare insets 6 and 7 in Fig. 4.3(a)). Vortex rows moving with different velocity is still possible (inset 7 in Fig. 4.3(b)). At larger currents different number of PSLs may collapse into one and the system transits to a higher resistive state (insets 9 and 10 in Fig. 4.3(a)). This kind of behavior of the moving vortex lattice has been found recently in Ref. [56] for the case of an infinite long wire. However, as a consequence of the nonuniform distribution of the superconducting current density near the normal leads, a finite curvature of the PSLs is found near the ends of the stripe (inset 8 in Fig. 4.3(a)). The latter is due to the fact that the moving vortices follow the contour line of maximal local current density where their velocity is maximal. Note that the effect of increased critical current j_{c2} disappears for this value of γ.

Fig. 4.3(b) show the I-V curve of the sample for $\gamma = 0$. At zero magnetic field (solid curve), regardless of the sample size, the system is in the full superconducting state at small applied currents (inset 1) and switches to the highly resistive state when the critical current density j_{c2} is reached (inset 2). Thus, for $\gamma = 0$, the system exists only in two phases (superconducting or normal) and there is no stable solution besides these two states at zero magnetic field. Previous studies using GL theory also indicated that the current range of such oscillatory phase-slip solutions diminishes with decreasing γ [56**?**]. At magnetic fields vortices exhibit chaotic motion with applying external current (inset 6). The vortex structure becomes spatially disordered before the PSL enters the sample, so that vortices will travel at different velocities across regions of the sample with unequal electric environment (inset 7). Contrary to the case of larger γ values, only giant phase slip lines can be stable for $\gamma = 0$.

Concluding this section, the superconducting-normal transition current j_{c2} increases with increasing γ. At the same time the effect of magnetic-field induced critical current enhancement becomes more pronounced at larger values of γ.

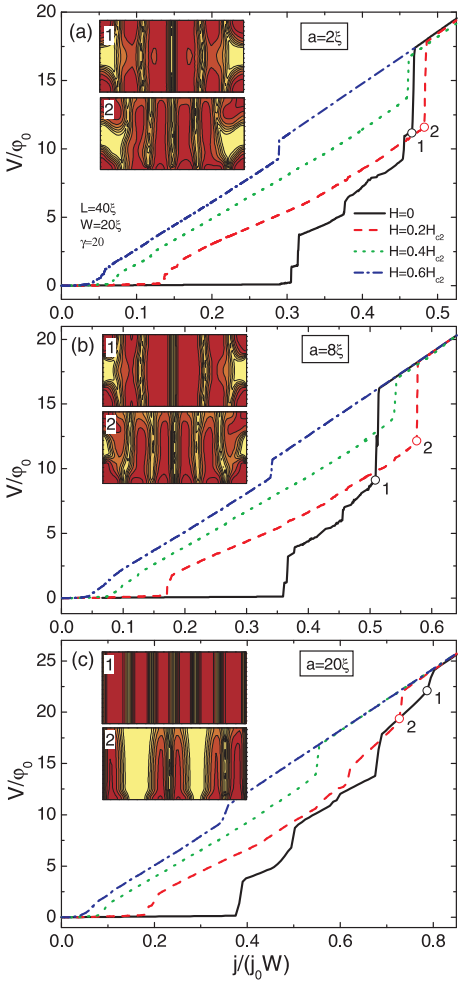

Fig. 4.4: The I-V curve of a superconducting stripe of width $W = 20\xi$ and length $L = 40\xi$ for different size of normal contacts: $a = 2\xi$ (a), $a = 8\xi$ (b) and $a = 20\xi$ (c) and for different magnetic fields. The insets show the Cooper-pair density plots at the magnetic field and current values indicated in the I-V curve.

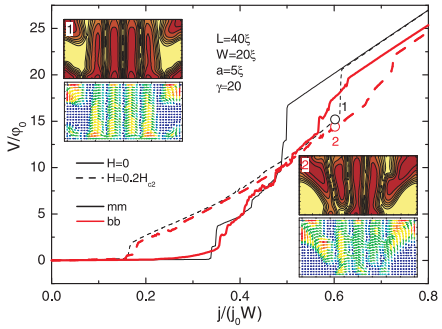

FIG. 4.5: The I-V curve of a superconducting stripe ($W = 20\xi$, $L = 40\xi$ and $\gamma = 20$) for $H = 0$ (solid curves) and $H = 0.2H_{c2}$ (dashed curves). The normal contacts ($a = 5\xi$) are attached in the middle of the sample side (thin curves) and on the bottom of the sample side (thicker curves). Insets show the Cooper-pair density plots (top figures) and vector plots of the superconducting current (bottom figures) for $j/(j_0W) = 0.58$, when the contacts are in the middle of the sample side (inset 1) and on the bottom of the sample side (inset 2).

4.5 THE INFLUENCE OF NORMAL CONTACTS

In most of the experiments devoted to the study of transport properties of superconducting samples, a microbridge geometry is used in order to reduce the power dissipation in the system. However, in the presence of an external magnetic field the bulk superconducting leads may turn into a normal state while the microbridge is still superconducting, which considerably changes the experimental picture. For example, the critical current of the superconducting nanowire can be significantly enhanced [85], as well as the critical current for the creation of phase slip centers can be affected [35] by the superconducting-normal transition of the leads. Thus, in most of the cases we have to deal with normal contacts. The presence of normal electrodes is in general closer to the real experimental situation, which may change the properties of the whole system in comparison with the solitary mesoscopic origin due to also possible quantum interference.

This motivated us to study the effect of the normal contacts on the transport properties of our sample. Fig. 4.4 shows the current-voltage characteristics of a stripe of size $L = 40\xi$ and $W = 20\xi$ for two different sizes of the normal leads. It is seen from this figure that, regardless of the size of the normal contact, the step structure of the I-V curve is preserved. Although different in the amplitude, the number of voltage jumps at zero magnetic field is independent on the size of the contacts a, i.e. the number of PSLs remains the same with increasing a (see inset 1 in Figs. 4.4(a-c)). However, the normal contact strongly influences the critical current for the transition from pure superconducting state

to the resistive state j_c and the critical current from finite resistive state to the normal state j_{c2}: both j_c and j_{c2} increases with increasing a. The reason for such increased critical current is as follows: due to the proximity effect superconducting order parameter is suppressed near the normal contacts, which means that the size of the sample is effectively decreased with increasing a. Smaller system sustains higher applied currents.

With applying magnetic field the jumps corresponding to appearance of extra phase slip lines vanishes, except the jumps corresponding to the entry of the first phase slip line and to the normal state transition. As in the case of zero magnetic field, j_c increases with increasing the size of the normal contacts. The effect of increased j_{c2} with applying small magnetic field has a nonlinear dependence on a. $j_{c2}(H)$-$j_{c2}(0)$ reaches its maximum at intermediate values of a (see also Fig. 4.2(d)) and decreases for larger (Fig. 4.4(c)) and smaller (Fig. 4.4(a)) values of a. Intermediate values of a prevent the formation of giant phase slip lines (see inset 2 in Figs. 4.4(a-c)). The fact that this field-induced critical current enhancement phenomenon vanishes for larger and smaller (e.g. bridge geometry) values on the contacts makes this effect difficult to be observed experimentally.

It turns out that the increase of j_{c2} with magnetic field is caused by the non-uniform distribution of currents in the sample due to the presence of normal contacts. To support this idea we conducted simulations when the normal contacts are attached in the middle of two sides of the sample (mm sample, see inset 1 in Fig. 4.5) and on the bottom of the sample (bb sample, inset 2 in Fig. 4.5). Fig. 4.5 shows the I-V curves of these two samples for $H = 0$ (solid curves) and $H = 0.2H_{c2}$ (dashed curves). As we see from this figure, j_{c2} for both values of the applied field considerably increases in the bb sample, where the strongly non-uniform distribution of the supercurrents is present (see the insets in Fig. 4.5). The latter means that the non-uniform distribution of currents plays an important role in the formation of stable resistive state.

Fig. 4.6 shows the value of the current at which point the system is driven to the normal state, i.e. the upper critical current density j_{c2} as a function of the applied magnetic field. For $\gamma = 0$ (dashed lines, open symbols), j_{c2} is a monotonically decreasing function of H for all values of a. j_{c2} is larger for larger size of the normal contacts a. For larger γ values (solid lines) there is a maximum in the $j_{c2}(H)$ curve. The height of this maximum is largest for intermediate values of a and vanishes for smaller and larger size of the normal contacts.

4.6 HYSTERETIC BEHAVIOR

It is known that the phase slip process in superconducting films is a hysteretic process (see e.g. Ref. [43]). If we start from the superconducting state and

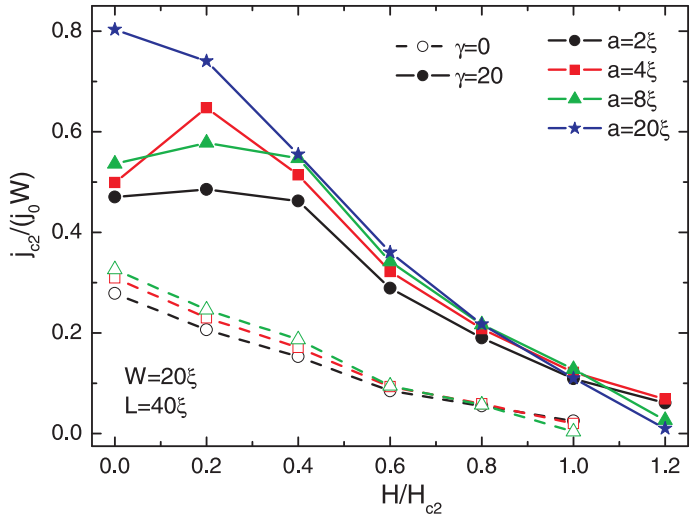

FIG. 4.6: Superconducting-Normal transition current density j_{c2} as a function of the applied field H/H_{c2} for different widths of the normal contacts a. Solid symbols represent the results obtained for $\gamma = 0$ and open symbols are the results for $\gamma = 20$. The size of the sample is $L = 40\xi$ and $W = 20\xi$.

gradually increase the applied current, the superconducting state becomes unstable and the system switches to the resistive superconducting or to the normal state at the upper critical current j_{c2}. The finite resistance can be due to moving vortices or phase slip lines as discussed in preceding sections. With decreasing current it is possible to keep the sample in this state for currents up to $j_{c1} < j_{c2}$. For $j < j_{c1}$ the phase slip solution cannot be realized (in the absence of fluctuations) and thus the current j_{c1} is the critical current where PSLs disappear.

Fig. 4.7 shows the current-voltage characteristics of a stripe with $L = 40\xi$ and $W = 20\xi$ for increasing (solid curves) and decreasing (dashed curves) transport currents for different values of the applied field H and the parameter γ. Let us first focus on the zero magnetic field case (black lines). As we mentioned above, for $\gamma = 0$ the system exhibits a transition from a fully superconducting state to a normal state at j_{c2} during the current sweep up. When we decrease the current starting from this value of the current, the sample becomes superconducting at j_{c1}. Thus the hysteretic loop is anticlockwise ($j_{c1} < j_{c2}$). For larger values of γ PSLs can enter the sample at currents $j_c < j_{c2}$. Therefore, we started from fully normal state during the current sweep down, in order not to affect the hysteresis loop [43]. The hysteretic loop $\Delta j = j_{c2} - j_{c1}$ is larger for larger γ (see the inset in Fig. 4.7) because of these phase-slip states.

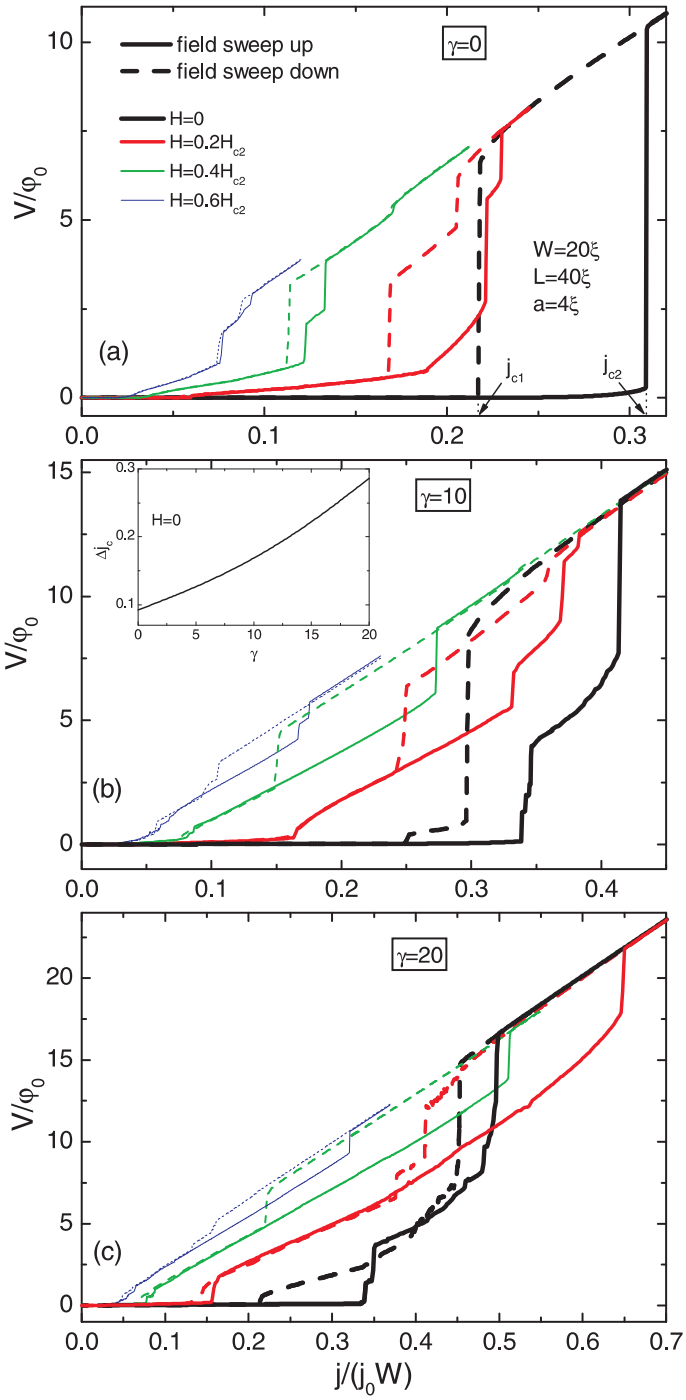

Fig. 4.7: Hysteresis in the I-V curve of the superconducting stipe with $L = 40\xi$ and $W = 20\xi$ for three different values of γ. Solid (dashed) curves show the results for current sweep up (down). The inset shows the width of the hysteretic loop for $H = 0$ as a function of γ.

The situation becomes more complicated when a magnetic field is applied to the sample. Because the number of possible states increases (see the previous section) and some of them become reversible for larger range of the applied current. For larger H the jumps in the I-V curves disappear and $V(I)$ turns to an almost smooth curve with strongly reduced hysteretic behavior (thinnest curves in Fig. 4.7).

4.7 CONCLUSION

Using the phenomenological TDGL formalism, we studied transport properties of thin superconducting stripes with attached normal leads in the presence of a perpendicular magnetic field. We found that at zero magnetic field finite resistance in the sample is brought by phase-slip lines. As the parameter γ increases the current range, over which such phase-slip state is possible, increases to higher and lower currents. Consequently, the superconducting normal transition current j_{c2} increases with increasing γ. But for $\gamma = 0$ no such oscillatory phase-slip solution exists at zero field. When a magnetic field is applied to the system, the number of distinct discontinuities in the I-V curve increases. This behavior is consistent with the restabilization of a moving vortex distribution by the formation of a dynamic vortex phase with distortion in the local flux density and vortex velocity. When the critical velocity of vortices is reached phase-slip lines appear across the sample. This phase-slip mechanism turns out to be more effective in producing resistance. The I-V curve exhibits a hysteretic behavior and the size of this hysteresis decreases with increasing magnetic field.

The most interesting result of our study is that for larger values of γ the normal state transition current j_{c2} increases with applying small external magnetic field as compared to j_{c2} at zero magnetic field. The reason for such magnetic field induced increase of the critical current is the nonuniform distribution of currents along the sample (due to the presence of normal contacts), which keeps the system in a resistive state for larger values of the applied current.

- A. K. Elmurodov, G. R. Berdiyorov, D. Y. Vodolazov, and F. M. Peeters, *Finite size effect on the resistive state in a mesoscopic type-II superconducting stripe* (in preparation).

5

The break-up of the vortex structure in a mesoscopic wire containing a constriction

5.1 INTRODUCTION

In recent years flat mesoscopic superconducting (SC) structures have been studied intensively both experimentally [86] and theoretically [87]. Unexpected new physics was found in superconducting Al disks, where the qualitative behavior of the magnetization (M) as a function of the magnetic field (H) was a sensitive function of the disk radius R: for very small radius of the sample the magnetization was continuous, for intermediate values of the disk radius a discontinuous $M-H$ behavior was observed with a single jump as in type-I SC and for larger radius of the disk multiple jumps are present in the magnetization, which is close to the behavior observed for bulk type-II superconductors. Note that bulk Al is a type-I superconductor. A theoretical investigation of the vortex structure in such disks based on the Ginzburg-landau (GL) theory predicted [88] that in such disks the vortices can coalesce into a single giant vortex or into single vortices dependent on the relative size, i.e. $R/\xi(T)$, and applied magnetic field ($\xi(T)$ is the temperature dependent coherence length). The transition between the giant to multi vortex state is of second order, as was recently confirmed experimentally [89].

The above systems are in essence two-dimensional (2D), i.e. the Cooper pair density does not vary along the thickness of the disk. The other limit of SC wires has also been investigated both theoretically [90] and experimentally [91].

As long as the wire is homogeneous the vortex structure will not vary along the wire and finding the spatial location of the vortices is a two-dimensional (2D) problem. Also in this case giant and multi-vortex configuration have been predicted. Since the type of vortex state which nucleate depends crucially on the relative thickness of the wire, i.e. $R/\xi(T)$, one may wonder what will happen with the vortex structure in a SC wire with variable thickness. For example, at the region where the width is sufficiently large N vortices penetrate the wire at a specific magnetic field while in the narrow region of the wire only $N^{'} < N$ vortices can be stabilized. How will this transition from N to $N^{'}$ vortices occur? Because the nucleation of a giant vortex state is very sensitive on the wire width, one can imagine that in a certain region of the wire one has a giant vortex while in a wider area of the wire multi-vortices are found. The splitting of a giant vortex into single vortices is a new phenomena which has not been investigated up to now.

To address the above physical phenomena we consider a model SC square wire which contains locally a constriction (see Fig. 5.1). The system we will investigate is related to a recently fabricated device where transport through a core shaped superconducting scanning tunnel microscope (STM) tip was investigated. [92–94] In order to explain some of these experimental results, Misko *et al.* [95] considered a conoidal geometry. They found that superconductivity survives in the narrowest part of the SC at magnetic fields much larger than the critical field of the bulk material. This is a direct consequence of surface superconductivity which is enhanced at sharp corners or at small areas of the SC [96]. Unfortunately, their approach did not allow for states with nonzero vorticity. They assumed cylindrically symmetric solutions, which, cannot give the correct vortex configuration in this geometry.

5.2 THEORETICAL MODEL

We apply the non-linear Ginzburg-Landau equations to describe the behavior of the order parameter as function of the applied magnetic field, which is taken in the z-direction,

$$(\bigtriangledown - iA)^2\psi + (1 - |\psi|^2)\psi = 0. \tag{5.1}$$

In Eq. (5.1) distance is scaled in units of the temperature dependent coherence length $\xi(T)$, the order parameter is in units of $\sqrt{\alpha/\beta}$, with α, β being the GL coefficients, and the magnetic field is in units of the second critical field $H_{c2}(T)$. We used the boundary condition $\left(-i\vec{\nabla}_{2D} - \vec{A}\right)\Psi\Big|_n = 0$ at the edge of the wire and superconducting normal metal boundary condition $\psi(0) = 0, \psi(L) = 0$ at the top and bottom of the sample.

The region of applicability of the stationary Ginzburg-Landau equation Eq. (5.1) is rather large, especially for 'dirty' superconductors where the mean free

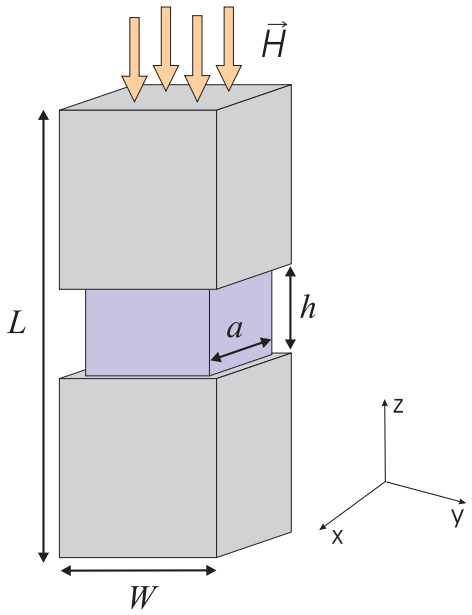

Fig. 5.1: Schematic picture of the mesoscopic superconducting wire.

path length l is much smaller than the coherence length $\xi_0 \sim v_F/\Delta(0)$ (Δ_0 is the superconducting gap at $T = 0$ and v_F is the velocity of electrons at the Fermi surface). They are valid in the limit $\xi(0) \ll \xi(T)$ which is satisfied pretty well for $0.9T_c < T < T_c$. Moreover, it was found that the formal application of the Ginzburg-Landau equations, when investigating the vortex structure in mesoscopic superconductors, gives quantitative agreement with experiment even for $T \to 0$ [87, 89]. Because the majority of microscopic and nanosize superconductors are in the 'dirty' limit, we expect that our results are applicable over a large range of temperatures and sizes of the SC. We will also neglect screening effects which is a reasonable approximation for 'dirty' superconductors where the London penetration depth λ is much larger than the coherence length. Therefore, even for a sample with size of several ξ the magnetic field inside the mesoscopic superconductor is approximately equal to the applied one and consequently we may neglect the second GL equation. Quantitatively it means that we chose $\xi < a \ll \lambda$ (see Fig. 5.1).

To solve Eq. (5.1) numerically we discretised the spatial coordinates and implemented the Euler method. The grid size was typically 0.5ξ in all directions. Decreasing the grid step resulted only in small quantitative changes, but did not influence the qualitative features and the interesting physics which we found. As an example, we took in our calculations $L = 50\xi$, $W = 6\xi$,

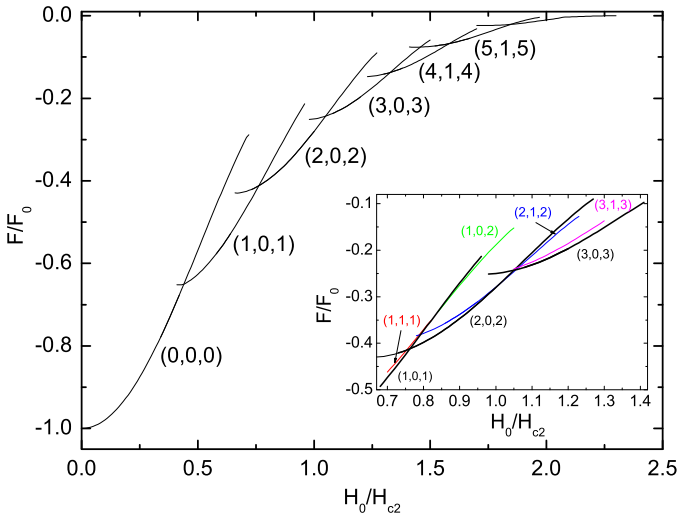

FIG. 5.2: The free energy of a nanowire with a construction as a function of the applied magnetic field for $W = 6\xi$, $L = 50\xi$, $a = 4\xi$, $h = 10\xi$ (see Fig. 5.1). The vortex state is characterized by three numbers: (n_t, n_m, n_b) which refer, respectively, to the vorticity in the top, middle and bottom part of the wire (see Fig. 5.1). The inset shows an enlargement of the intermediate magnetic field region with the metastable states shown in colour.

$a = 4\xi$ and $h = 10\xi$. Magnetic field is applied in the z direction and the vector potential is expressed in the symmetric gauge $\mathbf{A} = (-Hy/2, Hx/2, 0)$.

5.3 RESULTS AND DISCUSSIONS

When we apply a magnetic field the order parameter is more strongly suppressed in the widest parts because the induced screening current $\mathbf{j}_s = -|\psi|^2\mathbf{A}$ is larger there than in the more narrow part. The Meissner state becomes unstable for $H \simeq 0.6H_{c2}$ at which point two vortices enter the top, and bottom part of the SC wire while keeping the constriction free of vortices. Actually in our system the surface barrier effects are very strong, which is the reason for the large stability range of the metastable states. In Fig. 5.2 we plot the dependence of the free energy of our system for different vortex configurations where the vortex state is indicated as (n_t, n_c, n_b) where n_t (n_c, n_b) refers to the

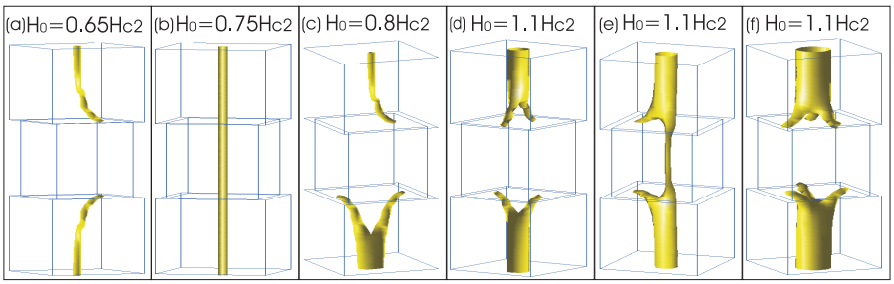

Fig. 5.3: Three dimensional isosurfaces of the Cooper-pair density at different magnetic fields and for different vortex configurations: (a) (1,0,1), (b) (1,1,1), (c) (1,0,2), (d) (2,0,2), (e) (2,1,2) and (f) (3,0,3).

number of vortices in the top (constriction, bottom) area of the SC wire. The 3D contour plots of the corresponding order parameter (vortex) distribution are depicted in Fig. 5.3.

Notice that nonsymmetric vortex states, with respect to $z = 0$ may exist in our system as metastable states. For example, the vortex state (1,0,2) is metastable and has a higher energy than the symmetric vortex configuration (see inset in Fig. 5.2). The surface barrier for vortex entry/exit is responsible for the strong hysteresis which is an intrinsic property of our wire. For example when we sweep down the magnetic field it is quite difficult to expel a vortex from the construction when it is present. It leads to the stability of such a state up to $H \simeq 0.7H_{c2}$ although energetically this state becomes unfavorable already at $H \simeq 1.3H_{c2}$.

Another interesting property of our system appears at large magnetic fields. At $H > 1.2H_{c2}$ the multi-vortex state can no longer be sustained in the wide parts of the wire and it transits to the giant-vortex state. When this giant vortex approaches the construction it splits into several vortices, because superconductivity is enhanced in the construction and the giant vortex is no longer stable (or metastable) here. As a result the giant vortex splits into multi-vortices near the construction where some vortices exit the sample (see Fig. 5.4). Near the constriction, but still in the upper part of the wire, the giant vortex $L = 3$ breaks up into a single vortex in the center and a $L = 2$ giant vortex which is displaced towards the edge of the wire (see Figs. 5.4(f,g)). The latter two vortices moves out of the system at the edge of the constriction. The contour plots of the phase for $H = 1.3H_{c2}$ show that in the upper thick part of the wire (see Fig. 5.4(d)) we have a giant vortex with vorticity $L = 3$ and in the constriction (Fig. 5.4(e)) only one vortex is present. This spatial break up of the giant vortex state into multi-vortices has not been predicted before.

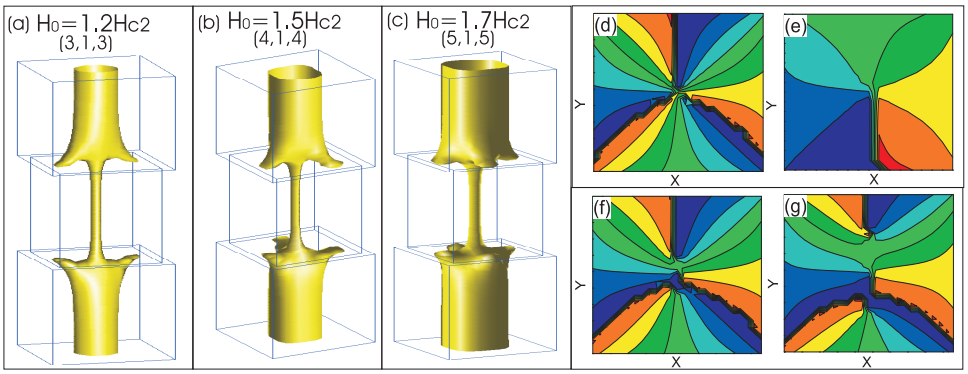

FIG. 5.4: Three dimensional isosurfaces of the suppressed Cooper-pair density in the region $H \geq 1.2H_{c2}$. Contour plots of the phase of the order parameter at the top (d), in the construction (e) and at the bottom of the wire are shown for the metastable vortex state (3,1,3) for $H = 1.3H_{c2}$: f) $z = 7\xi$ above the construction and g) $z = 0.5\xi$ just above the constriction.

5.4 CONCLUSION

In conclusion, we investigated vortex states in a nonuniform rectangular wire using the Ginzburg-Landau equation for the distribution of the order parameter (pairing potential of the Cooper pairs). Although we presented numerical results only for one specific set of parameters we found that the new physics is representative and typical for wires containing a local constriction. Namely, in a system where the constriction has a size less or comparable to the coherence length, the vortex cannot enter the construction (there is not enough space for it). Therefore, vortices nucleated in the widest part of the sample will be forced to be curved and exit the sample before reaching the constriction. At high magnetic field it will lead to the splitting of the giant vortex into a smaller giant or a multi-vortex state in the constriction region. Because of the inevitable presence of a surface barrier the development of the vortex structure is a hysteretic process and it depends on the preceding history of the variation of the applied magnetic field. The entrance and exit of vortices in the constriction should be reflected in the magnetoresistance and the magnetization of the sample.

- A. K. Elmurodov, D. Y. Vodolazov, and F. M. Peeters, *The break-up of the vortex structure in a mesoscopic wire containing a construction*, Europhys. Lett. **74**, pp 151-155 (2006)

6

Summary

The aim of this thesis was to study the nonstationary states in current-carrying superconducting samples. Such systems usually exhibit finite resistance when the current reaches to its critical value. The basic mechanism for such resistive stat – single phase-slip center – seems to be well understood: There is a periodic collapse and subsequent re-establishment of the order parameter in the core of a phase-slip center. The relaxation oscillation repeats with the Josephson frequency. In each collapse the difference across the filament is reduced by 2π. This leads to a stationary state, because this phase-slip mechanism leads to a phase loss which is equal to the increase of the phase difference during the phase-slip cycle. During each phase-slip cycle nonequilibrium quasiparticles are generated creating a charge imbalance on both sides of the phase-slip center. The diffusion and relaxation of these nonequilibrium quasiparticles are governed by the quasiparticles currents flowing through the phase-slip center which develops a voltage.

First we started with 1D superconducting wires, where we studied theoretically the effect of time symmetric and asymmetric electromagnetic (e. m.) radiation on the phase-slip process in superconducting wires in the regime where there is no stimulation of superconductivity. We found that for large amplitudes j^{ac} of the symmetric ac signal the value of the lower critical current $j_{c1}(j^{ac})$ at which the voltage vanishes in the sample oscillates as a function of j^{ac}. The amplitude of these oscillations decays with increasing power of the

ac signal, and we explain it either by the existence of a maximal current j_{c3} beyond which no phase slips can be created or by a weak heat removal from the sample. Applying an asymmetric in time signal (with zero *dc* current) we show that it may lead to a finite voltage in the system (i.e., ratchet effect). At high enough frequencies the rectified voltage is directly proportional to the frequency of the applied e.m. radiation. These properties resemble in many aspects the behavior of a Josephson junction under e.m. radiation. The differences are mainly connected to the effect of the transport current on the magnitude of the order parameter. We also showed that if the applied signal is asymmetric in time, it may lead to a ratchet effect as was shown in recent experiments Ref. [63] on annular Josephson junctions.

In the next chapter we investigated experimental and theoretical results on current-voltage characteristics of mesoscopic superconducting NbN wire. Different attached leads (superconducting contacts) allowed us to measure current-voltage (I-V) of different segments of the wire independently. The experimental results show that with increasing the length of the segment the number of jumps in the I-V curve increases indicating an increasing number of phase-slip phenomena. Recently experiments on superconducting nanowires [77] have attracted renewed attention on the elecrical and magnetic manifestations of thermal and quantum fluctuations. The successive nucleation of PSC leads to the appearance of a stairlike structure in the I-V characteristics [32, 33]. The existence of phase-slip centers was confirmed in low temperature superconductors [78]. Recently phase-slip centers were observed [79] in the presence of an external applied magnetic field. It was shown in Ref. [80] that with attaching many low-resistance Ohmic contacts along the electrodeposited Sn nanowires one can perform electrical measurements on different segments of the superconducting wire. It is often pointed out that phase-slip lines in wide films are similar to phase-slip centers in narrow films [81, 82]. The interpretation of the experimental results are supported by theoretical simulations that are based on the time dependent Ginzburg-Landau theory, coupled to the heat equation.

In chapter 4, we studied the creation of phase slip lines and the interplay with a vortex lattice in finite size superconducting thin films. With increasing applied current we show that the moving vortex lattice changes its structure from a triangular one to a set of parallel vortex rows in a pinning free superconductor. This effect originates from the change of the shape of the vortex core due to non-equilibrium effects (similar to the mechanism of vortex motion instability in the Larkin-Ovchinnikov theory). The moving vortex creates a deficit of quasiparticles in front of its motion and an excess of quasiparticles behind the core of the moving vortex. This results in the appearance of a wake (region with suppressed order parameter) behind the vortex which attracts other vortices resulting in an effective direction-dependent interaction between vortices. When the vortex velocity ν reaches the critical value ν_c quasi-phase slip lines (lines with fast vortex motion) appear which may coexist with slowly moving vortices between such lines. Our results were obtained within the framework

of the time dependent Ginzburg-Landau equations and are strictly valid when the coherence length $\xi(T)$ is larger or comparable with the decay length L_{in} of the non-equilibrium quasiparticle distribution function. In Refs. [53, 54] two types of vortex motion were found: slow and fast vortex motion (the latter was named the kinematic vortex [54]). However, neither the influence of the magnetic field nor the transition between these types of motion nor the transformation of the vortex lattice were addressed. In Ref. [55] the deformation of the vortex core due to the finite relaxation time of the order parameter was found and a short range attraction between vortices was predicted. In a recent paper [56] the rearrangement of the vortex lattice due to the above effect and the transition from the slow to the fast vortex motion (phase slip line) were studied for an infinitely long superconducting slab placed in a parallel magnetic field. We found the remarkable result that the normal state transition current increases at small applied magnetic field. This effect becomes more pronounced for larger values of the γ parameter in the GL formalism. We explained this unusual "field-induced" increase of the critical current by the nonuniform distribution of the currents in the sample.

In chapter 5 we studied the superconducting state in a mesoscopic wire containing a narrow constriction in the presence of a uniform magnetic field directed along the wire. If the narrow region is small enough so that no vortices can penetrate through it, curved vortices are formed i.e. they enter at the top of the sample (the widest part) and exit near the constriction. At high magnetic fields a giant vortex is nucleated in the widest part of the wire which breaks up into a smaller giant and/or individual vortices near the constriction.

7

Sumenvatting

In deze thesis onderzochten we de eigenschappen van phase-slip centra in supergeleiders waarop een nanostructuur is aangebracht.

Het basismechanisme achter een enkel phase-slip centrum (hetwelk de eerste potentiaalstap in een karakteristiek veroorzaakt) is reeds begrepen: In de kern van het fase-slip centrum vindt er een periodische opeenvolging van ineenstorten en heropbouwen van de orde parameter plaats. De relaxatie oscillatie herhaalt zich met de Joseshson frequentie. Tijdens elke ineenstorting wordt het verschil langsheen het filament gereduceerd door een factor 2π. Dit leidt tot een tijdsonafhankelijke toestand, doordat dit phase-slip mechnisme een fase verlies bewerkstelligt hetwelk gelijk is aan het toegenomen fase-verschil opgebouwd gedurende de phase-slip cyclus. Tijdens elke phase-slip cyclus worden er quasi-deeltjes gegenereerd, deze creëren een ladingsonevenwicht aan beide kanten van het phase-slip centrum. De diffusie en relaxatie van het onevenwicht van de quasi-deeltjes worden teweeggebracht door de stroom quasi-deeltjes doorheen het fase-slip centrum, deze geeft aanleiding tot een spanningsverschil.

In het tweede hoofdstuk onderzochten we theoretisch de invloed van tijdssymmetrische en -asymmetrische elektromagnetische (e. m.) straling op phase-slip processen in supergeleidende draden in het regime waarbij de supergeleiding niet gestimuleerd wordt. We vonden voor grote amplitudes j^{ac} van het symmetrische ac signaal dat de waarde van de laagste kritische stroom $j_{c1}(j^{ac})$, waarbij het voltageverschil verdwijnt in het sample, oscilleert als functie van

j^{ac}. De amplitude van deze oscillatie verdwijnt met het verhogen van het vermogen van het ac signaal, dit kunnen we verklaren ofwel door aanname van een maximale stroom j_{c3}, waarboven geen fase-slips kunnen gecreëerd worden, ofwel door een zwakke warmte afvoer uit het sample. Indien we een, in de tijd, asymmetrische signaal aanleggen (waarbij er geen dc stroom is) dan kan dit zoals we tonen leiden tot een eindig spanningsverschil over het systeem (d.i. het "ratchet effect). Bij voldoende hoge frequenties zal het spanningsverschil evenredig zijn met de frequentie van het aanglegde e.m. veld. De verschillen zijn hoofdzakelijk te wijten aan het effect dat de ladingstransport stromen hebben op de grote van de orde parameter. Tevens toonden we aan dat als het aangelegde signaal asymmetrisch is in de tijd dat dit kan leiden tot een "ratchet" effect zoals gevonden in recente experimenten op ring-vormige Josephson junctions, zie Ref. [63].

In het volgende hoofdstuk onderzoeken we de experimentele en theoretische resultaten van de stroom-spannings karakteristieken van een mesoscopische supergeleidende NbN-draad. Verschillende vastgemaakte leidingen (supergeleidende contacten), lieten ons toe de stroom-spanning (I-V) van verschillende delen van de draad onafhankelijk te meten. De experimentele resultaten tonen dat met het langer worden van de delen het aantal sprongen in de I-V curve toeneemt wat wijst op een verhoogd aantal fase-slip fenomenen. Onlangs hebben experimenten aan supergeleidende nanodraden [77] opnieuw de aandacht getrokken naar de elektrische en magnetische manifestaties van thermische en kwantumfluctuaties. De opeenvolgende nucleatie van PSC leidt tot het verschijnen van een trapachtige structuur in de I-V karakteristieken [32, 33]. Het bestaan van fase-slip centra werd bevestigd in lage temperatuur supergeleiders [78]. Onlangs werden fase-slip centra geobserveerd in de aanwezigheid van een uiwendig aangelegd magnetisch veld. In Ref. [80]werd aangetoond dat men door het bevestigen van veel lage-weerstands Ohmische contacten langs de elektrogedeponeerde Sn-draden elektrische metingen kan doen aan verschillende delen van de supergeleidende draad. Er wordt vaak op gewezen dat fase-slip lijnen in brede films gelijkaardig zijn aan fase-slip centra in dunne films [82**?**]. De interpretatie van de experimentele resultaten worden ondersteund door theoretische simulaties die gebaseerd zijn op de tijdsafhankelijke Ginzburg-Landau theorie, gekoppeld aan de warmtevergelijking.

In hoofdstuk 4 bestudeerden we de creatie van phase slip centra en de wisselwerking met een vortexrooster in dunne supergeleidende films van eindige grootte. Door het laten toenemen van de aangelegde stroom toonden we dat het bewegende vortexrooster de structuur verandert van driehoekig naar een set van parallele vortexrijen in een supergeleider zonder pinningscentra. Dit effect komt voort uit de verandering van de vorm van de vortexkern door niet-equilibrium effecten (gelijkaardig aan het mechanisme van vortexbewegingsinstabiliteit in de Larkin-Ovchinnikov theorie). De bewegende vortex creëert een tekort aan quasideeltjes voorop zijn beweging en een overschot van quasideeltjes achteraan de kern van de bewegende vortex. Dit resulteert in de verschijning van

een 'wake' (een gebied waarbinnen de ordeparameter onderdrukt wordt) achter de vortex die andere vortices aantrekt, wat aanleiding geeft tot een effectieve richtingsafhankelijke interactie tussen vortices. Wanneer de vortexsnelheid ν de kritieke waarde ν_c bereikt, verschijnen er quasi-phase slip centra (lijnen met snelle vortexbeweging) die samen kunnen bestaan met traag bewegende vortices tussen die lijnen. Onze resultaten werden verkregen binnen het kader van de tijsafhankelijke Ginzburg Landau theorie en zijn strikt geldig wanneer de coherentielengte $\xi(T)$ groter is dan of vergelijkbaar is met de vervallengte L_{in} van de distributiefunctie van het niet-equilibrium quasideeltje. In Ref. [53, 54] werden twee types vortexbeweging gevonden: trage en snelle vortexbeweging (laatsgenoemde wordt de kinematische vortex genoemd [54]). Echter, zowel de invloed van het magnetische veld, als de overgang tussen deze types van beweging, als de overgang van het vortexrooster werden niet behandeld. In Ref. [55] werd de deformatie van de vortexkern als gevolg van de eindige relaxatietijd van de ordeparameter gevonden en werd een korte-afstandsinteractie tussen vortices voorspeld. In een recent paper [56] werden de herinrichting van het vortexrooster door bovenstaand effect en de overgang van de trage tot de snelle vortexbeweging (phase slip centra) bestudeerd voor een oneindig lange supergeleidende plaat, geplaatst in een evenwijdig magneetveld. Dit effect wordt meer uitgesproken voor grotere waarden van de γ parameter in het GL-formalisme. We legden deze ongebruikelijke vorm van door het veld geïnduceerde supergeleiding uit door de afhankelijkheid van de de diffusielengte van de quasideeltjes van het magnetische veld.

In hoofdstuk 5 hebben we de supergeleidende toestand bestudeerd in een mesoscopische draad met een kleine vernauwing in de aanwezigheid van een magnetisch veld dat langs de draad is gericht. Als het nauwe gebied klein genoeg is, zodat er geen vortices door kunnen, worden er gebogen vortices gevormd, d.w.z ze komen binnen aan de bovenkant van het sample (de bredere gebieden) en gaan buiten in de buurt van de vernauwing. Bij hoge magnetische velden wordt er een grote vortex gevormd in het brede deel van de draad welke wordt opgedeeld in kleinere grote en/of individuele vortices in de buurt van de vernauwing.

List of abbreviations

(in alphabetic order)

Abbreviation or symbol	
B	Magnetic field
B_{cth}	Thermodynamical critical magnetic field
D	Diffusion constant
E	Electrical field
E_k	Quasiparticle excitation energy
e	Absolute value of the electron charge
$\hbar$	It is $\hbar = h/2\pi$, where h is Planck's constant
I	Total current
I_s	Supercurrent
j_c	Critical current density
j_n	Normal current density
L	Sample length
ℓ	Electron mean free path
m	Electron mass
N	Number of particles in a system (for instance electrons)
n	Electron density

Abbreviation or symbol

Q	Branch imbalance
Q^*	Charge Imbalance
T	Absolute temperature
T_c	Transition temperature at current I_c
T_{c0}	Critical temperature
t	Time
u	Normalization constant (TDGL)
V	Voltage
α	Constant of the Ginzburg-Landau theory
β	Constant of the Ginzburg-Landau theory
Γ	Pair-breaking parameter (GL theory)
γ	Pair-breaking parameter (TDGL theory)
$< \Delta >$	Average value of the gap
Θ	Debye temperature
Λ	Quasiparticle diffusion length
$\lambda(T)$	Magnetic penetration depth
μ	Electrochemical potential
μ_p	Electrochemical potential of Cooper pairs

Abbreviation or symbol	
$\xi(T)$	Ginzburg-Landau coherence length
σ	Conductivity in the normal state
τ	Scattering time in the normal state
τ_E	Inelastic electron-phonon collision time
τ_{PSC}	Period of the phase-slip process
$\varphi(\overrightarrow{r})$	Space dependent phase of the order parameter of the Gizburg-Landau
Ψ	Wave function
$\psi(\overrightarrow{r})$	Complex order parameter

References

1. H. Kamerlingh Onnes, Leiden Comm. **122b**, 124 (1911).
2. W. Meissner and R. Ochsenfeld, Naturwiss. **21**, 787 (1933).
3. J. G. Bednorz and K. A. Müller, Z. Phys. B **64**, 189 (1986).
4. US Department of Energy report (2006), *Basic Research Needs for Superconductivity*, *www.er.doe.gov/bes/reports/files/SC_rpt.pdf*.
5. A. V. Silhanek, L. Van Look, R. Jonckheere, B. Y. Zhu, S. Raedts, and V. V. Moshchalkov, Phys. Rev. B **72**, 014507 (2005).
6. P. A. Lee, N. Nagaosa, and X. G. Wen, Rev. Mod. Phys. **78**, 17 (2006).
7. J. S. Langer and V. Ambegaokar, Phys. Rev. **164**, 498 (1967).
8. D. E. McCumber and B. I. Halperin, Phys. Rev. B **1**, 1054 (1970).
9. F. Altomare, A. M. Chang, M. R. Melloch, Y. Hong, and C. W. Tu, Phys. Rev. Lett. **97**, 017001 (2006).
10. A. G. Sivakov, A. M. Glukhova, A. N. Omelyanchouk, Y. Koval, P. Muller, and A.V. Ustinov, Phys. Rev. Lett. **91**, 267001 (2003).
11. S. Khlebnikov and L. P. Pryadko, Phys. Rev. Lett. **95**, 107007 (2005).

12. W. J. Skochpol, M. B. Beasley, and M. Tinkham, J. Low Temp. Phys. **16**, 145 (1974).

13. J. D. Meyer, Appl. Phys. **2**, 303 (1973).

14. R. J. Watts-Tobin, Y. Krähenühl, and L. Kramer, J. Low Temp. Phys. **42**, 459 (1981).

15. L. Kramer and R. J. Watts-Tobin, Phys. Rev. Lett. **40**, 1041 (1978).

16. B. I. Ivlev and N. B. Kopnin, Sov. Phys. Uspekhi. **27**, 206 (1984), [Usp. Fiz. Nauk **142**, 435 (1984)].

17. W. A. Little, Phys. Rev. **156**, 396 (1967).

18. M. Tinkham, **Introduction to superconductivity** (McGraw Hill, New York, 1975).

19. B. D. Josephson, Phys. Lett. **1**, 251(1962).

20. T. J. Rieger, D. J. Scalapino, and J. E. Mercereau, Phys. Rev. B **6**, 1734 (1972).

21. J. D. Franson and J. E. Mercereau, J. Appl. Phys. **47**, 3261 (1976).

22. L. D. Jackel, R. A. Buhrman, and W. W. Webb, Phys. Rev. B **10**, 2872 (1974).

23. S. S. Pei, J. E. Lukens, and R. D. Sandell, Appl. Phys. Lett. B **36**, 88 (1980).

24. M. Tinkham, Festkörperprobleme (Adv. Solid State Phys.) XIX, 363, 1979).

25. A. B. Pippard, J. G. Shepherd, and D. A. Tindall, Proc. Roy. Soc. Lond. A **324**, 17 (1971).

26. G. J. Dolan and L. D. Jackel, Phys. Rev. Lett. **39**, 1628 (1977).

27. J. M. Aponte and M. Tinkham, J. Low Temp. Phys. **51**, 248 (1983).

28. M. Stuivinga, J. E. Mooij, and T. M. Klapwijk, J. Low Temp. Phys. **46**, 555 (1982).

29. R. Rangel and L. E. Guerrero, Phys. Rev. A **43**, 669 (1991).

30. M. Machida and H. Kaburaki, Phys. Rev. Lett. **71**, 3206 (1993).

31. I. Aranson and V. Vinokur, Phys. Rev. B **57**, 3073 (1998).

32. D. Y. Vodolazov, F. M. Peeters, L. Piraux, S. Matefi-Tempfli, and S. Michotte, Phys. Rev. Lett. **91**, 157001 (2003).

33. S. Michotte, S. Ma'te'fi-Tempfli, L. Piraux, D. Y. Vodolazov, and F. M. Peeters, Phys. Rev. B **69**, 094512 (2004).

34. D. Y. Vodolazov, F. M. Peeters, M. Morell, and V. V. Moshchalkov, Phys. Rev. B **71**, 184502 (2005).

35. D. Y. Vodolazov, Phys. Rev. B **75**, 184517 (2007).

36. J. Rubinstein, P. Sternberg, and Q. Ma, Phys. Rev. Lett. **99**, 167003 (2007).

37. A. A. Abrikosov, Sov. Phys. JETP **5**, 1174 (1957).

38. A. I. Larkin and Yu. N. Ovchinnikov, Zh. Eksp. Teor. Fiz. **68**, 1915 (1975), [Sov. Phys. JETP **41**, 960 (1976)]; A. I. Larkin and Yu. N. Ovchinnikov, in *Nonequilibrium Superconductivity*, edited by D.N. Langenberg and A.I. Larkin (North-Holland, Amsterdam, 1986), p.493.

39. W. Klein, R. P. Huebener, S. Gauss, and J. Parisi, J. Low Temp. Phys. **61**, 413 (1985).

40. L. E. Musienko, I. M. Dmitrenko, and V. G. Volotskaya, Pisma Zh. Eksp. Teor. Fiz. **31**, 603 (1980) [JETP Lett. **31**, 567 (1980)]

41. D. Babic, J. Bentner, C. Surgers, and C. Strunk, Phys. Rev. B **69**, 092510 (2004).

42. M. Tian, J. Wang, J. S. Kurtz, Y. Liu, M. H. W. Chan, T. S. Mayer, and T. E. Mallouk, Phys. Rev. B **71**, 104521 (2005).

43. A. V. Samoilov, M. Konczykowski, N. C. Yeh, S. Berry, and C. C. Tsuei, Phys. Rev. Lett. **75**, 4118 (1995).

44. S. G. Doettinger, R. P. Huebener, R. Gerdemann, A. Kuhle, S. Anders, T. G. Trauble, and J. C. Villegier, Phys. Rev. Lett. **73**, 1691 (1994).

45. S. G. Doettinger, S. Kittelberger, R. P. Huebener, and C. C. Tsuei, Phys. Rev. B **56**, 14157 (1997).

46. Z. L. Xiao and P. Ziemann, Phys. Rev. B **53** 15265 (1996).

47. Z. L. Xiao, P. Voss-de Haan, G. Jakob, Th. Kluge, P. Haibach, H. Adrian, and E. Y. Andrei, Phys. Rev. B **59** 1481 (1999).

48. A. E. Koshelev and V. M. Vinokur, Phys. Rev. Lett. **73** 3580 (1994).

49. J. A. Fendrich, U. Welp, W. K. Kwok, A. E. Koshelev, G. W. Crabtree, and B. W. Veal, Phys. Rev. Lett. **77** 2073 (1996).

50. Z. L. Xiao, E. Y. Andrei, and P. Ziemann, Phys. Rev. B **58**, 11185 (1998).

51. M. N. Kunchur, Phys. Rev. Lett. **89** 137005 (2002).

52. S. V. Lempitskii, Zh. Eksp. Teor. Fiz. **90**, 793 (1986) [Sov. Phys. JETP **63**, 462 (1986)].

53. A. Weber and L. Kramer, J. Low Temp. Phys. **84**, 289 (1991).

54. A. Andronov, I. Gordion, V. Kurin, I. Nefedov, and I. Shereshevsky, Physica C **213**, 193 (1993).

55. L. I. Glazman, Fiz. Nizk. Temp. **12**, 688 (1986) [Sov. J. Low Temp. Phys. **12**, 389 (1986)].

56. D. Y. Vodolazov and F. M. Peeters, Phys. Rev. B **76**, 014521 (2007).

57. R. Kato, Y. Enomoto, and S. Maekawa, Phys. Rev. B **47**, 8016 (1993).

58. B. I. Ivlev, G. Lisitsin, and G. M. Eliashberg, J. Low Tenp. Phys. **10**, 449 (1973).

59. S. Shapiro, Phys. Rev. Lett. **11**, 80 (1963).

60. A. G. Sivakov, A. M Glukhov, A. N. Omelyanchouk, Y. Koval, P. Müller, and A. V. Ustinov, Phys. Rev. Lett. **91**, 267001 (2003).

61. R. Tidecks, *Current-induced Nonequilibrium phenomena in quasi-one-dimensional superconductors*, pp. 1-134, Springer-Verlag, Berlin-New York (1990).

62. A. Barone and G. Paterno, *Physics and Applications of the Josephson Effect* (Wiley, New York, 1982), Chap. 11.

63. A. V. Ustinov. C. Coqui, A. Kemp, Y. Zolotaryuk, and M. Salerno, Phys. Rev. Lett. **93**, 087001 (2004).

64. A. V. Gurevich and R. G. Mints, Rev. Mod. Phys. **59**, 941 (1963).

65. B. I. Ivlev and N. B. Kopnin, Adv. Phys. **33**, 47 (1984).

66. J. A. Pals and J. Wolter, Phys. Rev. Lett. **70A**, 150 (1979).

67. The time between PS events, τ_{PS} is inversely proportional to the voltage via the Josephson relation $\tau_{PS} \sim 1/V$. Both for Josephson junctions and for phase-slip centers the voltage increases with applied current and hence the time τ_{PS} decreases.

68. Oscillations in the current j_{c1} starts to be pronounced when two PS events (one "positive" and one "negative") can be "fit" into a period of the electromagnetic radiation, which is proportional to the jump of the voltage $\triangle V$ at current j_{c1}: $\upsilon_c \simeq 2e\Delta V/\hbar$. The reason is that $\triangle V$ provides a lower threshold for the time between two PS events $\upsilon_c = \hbar/2e\Delta V$. When $\upsilon \ll \upsilon_c$ within a period $1/\upsilon$ many PS events occur and oscillations become invisible.

69. If one considers the underdamped case, then hysteresis and a finite-voltage jump will appear in the current-voltage characteristics of the Josephson junction and hence property (i) may appear. This limit should be investigated separately and is left for future investigation.

70. V. V. Schmidt, *The Physics of Superonductors* (Springer-Verlag, Berlin, 1997), Chap. 7.

71. J. Berger, Phys. Rev. B. **71**, 174504 (2005).

72. S. Flach, Y. Zolotaryuk, A. E. Miroshnichenko, and M. V. Fistul, Phys. Rev. Lett. **88**, 184101 (2002).

73. M. Salerno and Y. Zolotaryuk, Phys. Rev. E **65**, 056603 (2002).

74. D. N. Langenberg, D. J. Scalapino, B. N. Taylor, and R. E. Eck, Phys. Lett. **20**, 563 (1966).

75. J. T. Chen, R. T. Todd, and Y. W. Kim, Phys. Rev. B. **5**, 1843 (1972).

76. R. Tidecks, Springer Tracts in Modern Physics, Vol. **121**, Springer, Berlin (1990).

77. A. Bezryadin, C. N. Lau, M. Thinkham, Nature (London) **404**, 971 (2000).

78. Z. Zhou, R. J. Gyula, D. Mandris, V. Barzykin, P. Schlottman, Y. Hor, Z. Xiao, and J. F. Mitchell, Phys. Rev. B. **76**, 104511 (2007).

79. A. Falk, M. M. Deshmukh, A. L. Prieto, J. J. Urban, A. Jonas, and H. Park, Phys. Rev. B. **75**, 020501 (2007).

80. D. Lucot, F. Pierre, D. Mailly, K. Yu-Zhang, S. Michotte, F. de Menten de Horne, and L. Piraux, Appl. Phys. Lett. **91**, 042502 (2007).

81. V. G. Volotskaya, I. M. Dmitrenko, L. E. Musienko and A. G. Sivakov, J. Low Temp. Phys. **10**, 179 (1984).

82. V. I. Kuznetsov and V. A. Tulin, JETP Lett. **61**, 1026 (1995).

83. V. M. Dmitriev, I. V. Zolochevskii, T. V. Salenkova, and E.V. Khristenko, Low Temp. Phys. **31**, 127 (2005).

84. L.P. Gor'kov, Zh. Eksp. Teor. Fiz. **36**, 1918 (1959) [Sov. Phys. JETP **9**, 1364 (1959)].

85. M. Tian, N. Kumar, S. Xu, J. Wang, J. S. Kurtz, and M. H. W. Chan, Phys. Rev. Lett. **395**, 076802 (2005); M. Tian, N. Kumar, J. Wang, S. Xu, and M. H. W. Chan, Phys. Rev. B **74**, 014515 (2006).

86. A. K. Geim, I. V. Grigorieva, S. V. Dubonos, J. G. S. Lok, J. C. Maan, A. E. Filippov, and F. M. Peeters, Nature (London) **390**, 256 (1997).

87. Deo P. Singha, V. A. Schweigert, F. M. Peeters, and A. K, Geim, Phys. Rev. Lett. **79**, 4653 (1997) .

88. V. A. Schweigert, F. M. Peeters, and Deo P. Singha, Phys. Rev. Lett. **81**, 2783 (1998).

89. A. Kanda, B. J. Baelus, F. M. Peeters, K. Kadowaki, and Y. Ootuka, Phys. Rev. Lett. **93**, 257002 (2004).

90. G. Stenuit, S. Michotte, J. Govaerts, and L. Piraux, Eur. Phys. J. B **33**, 103 2003; G. Stenuit, S. Michotte, J. Govaerts, L. Piraux, and D. Bertrand, Mod. Phys. Lett. **B17**, 537 (2003); G. Stenuit, S. Michotte, J. Govaerts, and L. Piraux Supercond. Sci. Technol. **18**, 174 (2005).

91. S. Michotte, L. Piraux, S. Dubois, F. Pailloux, G. Stenuit and J. Govaerts, Physica C **377**, 267 (2002).

92. M. Poza, E. Bascones, J. G. Rodrigo, N. Agrait, S. Vieira, and F. Guinea, Phys. Rev. B **58**, 11173 (1998).

93. H. Suderow, E. Bascones, A. Izquierdo, F. Guinea, and S. Vieira, Phys. Rev. B **65**, 100519(R) (2002).

94. J. G. Rodrigo, H. Suderow, and S. Vieira, Physica Status Solidi B **1**, 386 (2003).

95. V. R. Misko, V. M. Fomin. and J. T. Devreese, Phys. Rev. B **64**, 014517 (2001).

96. V. A. Schweigert, and F. M. Peeters, Phys. Rev. B **60**, 3084 (1999).

Curriculum Vitae

Elmurodov Azamat

Born on April 29, 1977
in Qashqadaryo / Uzbekistan

September 1994 - June 1998: Bachelor's Diploma in Mathematics, Samarkand State University, Samarkand, Uzbekistan.

July 1999 - September 2001: Master's Diploma in Mathematics, Samarkand State University, Samarkand, Uzbekistan.

Promotor: Prof. dr. F. M. Peeters
Co-promotor: Dr. D. Yu. Vodolazov

Scientific award

2005 The best poster presentation in Joint International Workshop on "Arrays of Quantum Dots and Josephson Junctions (AQDJJ)", 9-25 June 2005, Kiten, Bulgaria.

List of publications

1. D. Y. Vodolazov, A. K. Elmurodov, and F. M. Peeters, *Critical currents of the phase slip process in the presence of electromagnetic radiation: Rectification for time assymetric ac signal*, Phys. Rev. B **72**, 134509 (2005).

2. A. K. Elmurodov, D. Y. Vodolazov, F. M. Peeters, S. Michotte, S. Adam, F. de Menten de Horne, L. Piraux, D. Lucot, D. Mailly, *Phase-slip phenomena in NbN superconducting nanowires with leads* (submitted to Phys. Rev. B.).

3. A. K. Elmurodov, G. R. Berdiyorov, D. Y. Vodolazov, and F. M. Peeters, *Conversion of vortex lines into phase slip lines in thin wide superconducting strips of finite length: implication for the I-V response* (in preparation).

4. A. K. Elmurodov, D. Y. Vodolazov, and F. M. Peeters, *The break-up of the vortex structure in a mesoscopic wire containing a construction*, Europhys. Lett. **74**, pp 151-155 (2006).